THESIS

# TWO DISTINCT LINEAGES OF *PANTOEA ANANATIS* ARE DIVERGENT IN TOXIN PRODUCTION POTENTIAL AND HOST SPECIALIZATION

Submitted by

Mitchell Quentin Giebler

Department of Agricultural Biology

In partial fulfillment of the requirements

For the Degree of Master of Science

Colorado State University

Fort Collins, Colorado

Summer 2026

Master's Committee

Advisor: Jan E. Leach

Co-Advisor: Federico Martin

Robyn Roberts

Brad Borlee

# ABSTRACT

## TWO DISTINCT LINEAGES OF *PANTOEA ANANATIS* ARE DIVERGENT IN TOXIN PRODUCTION POTENTIAL AND HOST SPECIALIZATION

*Pantoea ananatis* has recently emerged as a causal agent of *Pantoea* leaf blight of rice in the United States, raising concerns about its potential impact on rice production. Despite increasing reports of the disease, the mechanisms underlying host specialization and virulence within this pathosystem remain poorly understood. Here, comparative genomics and *in-planta* assays are combined to investigate population structure and virulence determinants among rice-associated *P. ananatis* strains. Average nucleotide identity analysis of *P. ananatis* genomes resolved two distinct lineages with contrasting host associations. One lineage, composed of strains recovered exclusively from rice, lacked the HiVir operon responsible for synthesis of the phosphonate toxin pantaphos. A second, more broadly distributed lineage included *P. ananatis* isolated from diverse hosts, including rice, and many contained the HiVir operon. HiVir-mediated pantaphos production drove necrotic symptom development in rice but was not required for bacterial replication within rice tissue. Accordingly, strains lacking HiVir, including those from the rice-associated lineage and targeted mutants, exhibited reduced necrosis while achieving bacterial population sizes comparable to wild-type generalist strains during infection of rice. Conversely, host-range experiments showed that rice-associated strains exhibited reduced colonization in onion tissue relative to generalist strains, consistent with evolutionary specialization to rice. Comparative pangenome analysis supported the evolutionary separation of these lineages and identified hundreds of lineage-specific genes, in-tact secretion systems, and secondary metabolite biosynthetic gene clusters that may underpin host associations. These findings demonstrate that

*P. ananatis* populations associated with rice comprise distinct evolutionary lineages with differing genomic features and virulence strategies and reveal a decoupling between symptom development and bacterial proliferation during infection of rice.

ACKNOWLEDGEMENTS

I would like to express a great deal of thanks to my advisor, Dr. Jan Leach. It was as an undergraduate in her lab that I first fell in love with science, largely because of how amazing the experience in her lab has been. Her steady encouragement and unwavering support have given me a foundation I will carry throughout my career. I simply could not have asked for a better mentor.

My co-advisor, Dr. Federico Martin, has generously given his time and expertise at every stage of this work. So much of what I know at the bench I owe to his patient teaching, offered selflessly despite many competing demands on his time. The rest of my committee, Dr. Brad Borlee and Dr. Robyn Roberts, have been a pleasure to collaborate with. Their expertise has been invaluable and their openness to discussion greatly appreciated during the duration of my degree.

Many Leach lab members are responsible for the friendly, welcoming environment that I have been lucky enough to call home. Dr. Emily Luna laid much of the groundwork for this project, but it is her remarkable kindness over the years has meant so much to me. Kamal Neupane has been my constant companion through thousands of hours at the bench, and I am lucky to count him among my closest friends.

Dr. Ana Cristina Fulladolsa gave me my first real opportunity in science as an undergraduate. She opened a door to a world I didn't know existed and has always encouraged me to explore it with enthusiasm.

My path towards graduate research would not have been possible without my family. My mother Holli, my father Michael, and my sister Claudia have been a constant source of love and support, always there when I needed to lean on someone. I love you all.

Finally, my partner Grace has walked alongside me through every step of graduate school. She is my ultimate supporter my best friend. I love you.

TABLE OF CONTENTS

# CHAPTER 1: LITERATURE REVIEW

## The many lifestyles of *Pantoea ananatis*

*Pantoea ananatis,* a yellow-pigmented bacterium in the family Enterobacteriaceae, is remarkable for its ability to thrive in different ecological niches (Coutinho and Venter 2009). It has been isolated as a free-living bacterium, from soil, water, and air; from agricultural systems associated with both plants and insects; from human bacteremic infections; and from rather extreme environments, such as aviation fuel tanks (De Maayer et al. 2014; LaGier et al. 2022; Luhung et al. 2018; Pileggi et al. 2012; Rauch et al. 2006)

The ecological diversity and cross-kingdom host range of this species is often attributed to vast genomic plasticity. Pan-genomic analyses of *P. ananatis* have revealed a core genome, consisting of genes shared between all isolates, and an open pan-genome, with new accessory genes discovered each time a new genome is sequenced (Weller-Stuart et al. 2017a). The genomic differences between individual strains are thought to determine a strain's lifestyle, niche range, and ability to colonize plant, insect, and animal hosts (De Maayer et al. 2014).

Major drivers of this within-species genetic diversity are the integration of phage elements, which appear in all sequenced genomes, as well as integrative conjugative elements (ICEs) and other insertion sequences (De Maayer et al. 2014). In fact, in available genomes, thousands of horizontal gene transfer (HGT) signatures have been documented (Agarwal et al. 2021). *P. ananatis* also shows flexibility regarding the genetic content of its genus-wide conserved plasmid, large *Pantoea* plasmid (LPP-1), and can harbor several additional accessory plasmids of various sizes (De Maayer et al. 2012; Weller-Stuart et al. 2017a).

Even the role of *P. ananatis* as a plant-associated bacterium is ambiguous. Descriptions include asymptomatic associations, both endophytically, multiplying within plant tissue, and epiphytically, growing on plant surfaces (Gitaitis et al. 2002; Megías et al. 2016; Sheibani-Tezerji et al. 2015; Watanabe et al. 1996). In some asymptomatic associations, *P. ananatis* provides a beneficial role for the plant, promoting growth. These interactions have been linked to distinct characteristics of some strains: phosphate solubilization, enhancing phosphorus availability for the plant; indole acetic acid (IAA) production, a hormone with positive effects on plant growth; 1-Aminocyclopropane-1-carboxylic acid (ACC) deaminase production, degrading ACC, a precursor of ethylene that accumulates during stress; and siderophore production, increasing iron availability (Lu et al. 2021). Because of this, *P. ananatis* has enhanced rice growth in saline conditions, improved papaya root and shoot development, and helped increase tomato biomass (Duchateau et al. 2025; Lu et al. 2021; Thomas et al. 2007). Inoculations with beneficial strains of this species have also induced plant systemic resistance to *Xanthomonas axonopodis* pv. *vesicatoria* in pepper, and *P. ananatis* strains have shown direct antagonism toward the known plant pathogens *Xanthomonas oryzae* pv. *oryzae, Erwinia amylovora,* and *Botrytis cinerea* (Gasser et al. 2012; Kang et al. 2007; Lee et al. 2024; Tian et al. 2026).

The emergence of *P. ananatis* as a pathogen itself, however, is of particular concern. Originally described causing brown rot of pineapple in the Philippines (Serrano 1928), it has since been described causing disease on numerous plant hosts (Coutinho and Venter 2009). Moreover, the geographical spread of this pathogen has breached all continents, excluding Antarctica, causing significant yield penalties and post-harvest losses (Bragard et al. 2023). Despite its widespread reach, relatively little is known about the pathogenic nature of *P. ananatis* relative to other phytopathogenic bacteria.

## Emergence of *P. ananatis* as a pathogen of rice in the United States

Emergence of *P. ananatis* on rice in the United States (USA) is a recent and evolving issue that raises concern for the country's southern rice belt. The first official report of *Pantoea* leaf blight in the USA occurred in research plots in Arkansas, observed in 14 of 570 global rice genotypes (Luna et al. 2023). Symptoms included spreading leaf lesions, panicle sterility, and reduced yield. Subsequently, in Louisiana, the pathogen was described causing panicle and leaf blight-like symptoms in variety PVL03 (Bruno et al. 2025). More recently, isolation of *P. ananatis* from both rice leaf and seed tissue in Arkansas has been confirmed, with each isolate displaying different degrees of aggressiveness (de Paula et al. 2026). *P. ananatis* has now appeared in commercial rice fields in Texas (Khanal et al. Unpublished).

*P. ananatis* has been observed as a plant pathogen on other hosts in the USA for decades, causing disease on onion, melon, sudangrass, maize, sorghum, wheat, cotton, and peanut (Alhusays et al. 2024; Arias et al. 2013; Azad et al. 2000; Gitaitis and Gay 1997; Medrano and Bell 2015; Obasa et al. 2024; Obasa et al. 2023; Wells et al. 1987). Despite this, its recent and erupting emergence on rice is alarming considering the significant contribution of rice production to the US economy (Wang et al. 2024), and the lack of knowledge of mechanisms of virulence within the rice system (Azizi et al. 2020).

## *P. ananatis* population structure

The emergence of *P. ananatis* in the rice system may be further complicated by its population structure. Recent phylogenetic analyses consistently revealed a two-clade organization within the species. One study demonstrated genetic differentiation between two clades with genome-wide metrics (De Maayer et al. 2017). Average nucleotide identity (ANI)

values between the clades were approximately 96-97%, supported with digital DNA-DNA hybridization (dDDH) values around 69%, which approaches the threshold for species demarcation. This genetic distinction between lineages provides support for divergent evolutionary trajectories. Interestingly, genomes from one clade, called clade 2, exhibited reduced variability in encoded proteins compared to the other clade (clade 1), potentially pointing to restricted niche inhabitation. The groups also were associated with differential plasmid content, with clade 1 typically harboring more plasmids than clade 2 (De Maayer et al. 2017).

These results were corroborated with another genomic analysis that revealed two subclades defined by high (above 98.5%) within clade ANI, but lower (approximately 97%) between clade ANI (Crosby et al. 2023). This study also identified gene content differences between clades, focusing on a few patterns, with two genes (one involved in ion transport, another a putative beta-carotene dioxygenase) enriched in clade1 and absent from clade 2. Clade 2 was represented by nine enriched genes (associated with cytochrome C, membrane proteins, and hypothetical proteins) that were absent from clade 1 (Crosby et al. 2023).

Multi-locus sequence analysis (MLSA) of five housekeeping genes (*fusA, gyrB, leuS, rpoB,* and *pyrG*) further supported the grouping of this species (Bing et al. 2022). Clade 2 was characterized by smaller average genome size (mean = 4.75 Mb for clade 2; 4.89 Mb for clade 1), reduced coding sequence content (mean = 4,266 for clade 2; 4,365 for clade 1), and higher pseudogene numbers (mean = 114 for clade 1; 98 for clade 2) compared to clade 1 (Bing et al. 2022). Eleven genomes were included in this analysis of clade 2, 10 of which were isolated from rice, suggesting evolution with rice over a long period of time (Bing et al. 2022).

Collectively, there is quite strong evidence for the distinction of two *P. ananatis* lineages, but the genes underlying these differences and the functional importance of the groupings and their host associations are poorly understood.

**Molecular determinants of virulence**

*Pantaphos*

Pantaphos, a small-molecule derivative of phosphonate, chemically identified as 2-(hydroxy[phosphono]methyl)maleate, represents the primary characterized virulence factor responsible for onion center rot disease caused by *P. ananatis* (Polidore et al. 2021). The discovery of pantaphos emerged from genetic studies that identified *pepM* as an essential gene for symptom development in onion (Asselin et al. 2018). Characterization of the role of *pepM* in phosphonate biosynthesis surfaced in 1988 (Bowman et al. 1988; Hidaka et al. 1989; Seidel et al. 1988) and has since been linked to nearly every bacterial phosphonate biosynthetic gene cluster (Ju et al. 2014). In *P. ananatis, pepM* is the first gene in an operon termed HiVir (Asselin et al. 2018), characterized by elements consistent with horizontal gene acquisition (flanked by putative transposases, low GC content) (Asselin et al. 2018). Subsequent analyses have confirmed the role of *pepM* (also termed *hvrA*), as well as the importance of other genes in the HiVir operon for the production of pantaphos and development of symptoms on onion (Polidore et al. 2024; Polidore et al. 2021; Shin et al. 2023).

Pantaphos has broad-spectrum toxicity to plants, with phytotoxic effects toward tobacco and mustard seedlings, in addition to onion (Polidore et al. 2021). The effect of pantaphos on mustard seedlings was comparable to that of commercial phosphonate-based herbicides (glyphosate and phosphinothricin), and interestingly, it exhibited moderate cytotoxicity against

human cancer cell lines. Because pantaphos showed no antibacterial or antifungal activity, there is suggested specificity for plants and animals, likely targeting metabolic processes shared between the two, but absent or sufficiently different in prokaryotes and fungi (Polidore et al. 2021).

While the specific molecular targets for pantaphos remain uncharacterized, structural analysis of the molecule has provided clues for its mode of action (Polidore et al. 2024). The compound bears resemblance to the common cellular metabolites isocitrate and isopropylmalate. This, combined with the fact that the proposed biosynthetic pathway follows similar chemical logic to the citric acid (TCA) cycle and leucine biosynthesis, suggests that pantaphos may interfere with central metabolic pathways of plants and animals (Polidore et al. 2024).

The proposed pathway begins with HvrA (PepM), which catalyzes an energetically unfavorable reaction that rearranges phosphoenolpyruvate (PEP) to phosphonopyruvate (PnPy). HvrC drives the pathway forward by condensing PnPy with acetyl-CoA to form 2-phosphonomethylmalate (PMM). In yet another thermodynamically unfavorable reaction, HvrD and HvrE form a heterodimeric dehydratase that catalyzes the dehydration of PMM to phosphonomethylmaleate (PMME). To overcome the unfavorable thermodynamics of the dehydration step, HvrF (S-adenosylmethionine (SAM)-dependent methyltransferase) irreversibly methylates PMME to form methyl-PMME, pulling the reaction forward. Next, HvrB (flavin-dependent monooxygenase) and HvrK (flavin reductase) use molecular oxygen to hydroxylate methyl-PMME, converting it to methylpantaphos. This is a precursor to pantaphos that is likely exported from the cell by HvrI (MFS transporter). A final step involving the hydrolysis of the methyl ester linkage to yield active pantaphos remains mechanistically unclear, although this

likely happens during transport out of the cell or in the extracellular environment (Polidore et al. 2024).

Systematic mutagenesis revealed differential contributions of individual HiVir genes to symptom development and pathogenicity in onion. Essential contributions were observed for genes *hvrA* through *hvrF*, consistent with their predicted roles in the core biosynthetic pathway. This was determined by measuring symptom development and bacterial enumeration after inoculation. Genes *hvrG* through *hvrJ* showed only partial contributions to pathogenicity, suggesting supporting roles in pantaphos production or modification. Notably, *hvrK* showed no detectable contribution to symptom development despite its predicted role as a flavin reductase (Shin et al. 2023).

Strains of *P. ananatis* can encode multiple distinct predicted phosphonate biosynthetic clusters in addition to HiVir. In fact, four predicted phosphonate clusters exist throughout analyzed *P. ananatis* genomes: the HiVir operon, which is most common; a predicted phosphonate biosynthetic gene cluster lacking *pepM,* named *Pgb,* that resembles a phosphonoglycan biosynthesis locus in *Glyomyces* sp. and two other clusters, both containing *pepM.* All genomes of *P. ananatis* also contain a gene cluster for phosphonate catabolism, deemed the *phn* locus (Polidore et al. 2021).

To characterize any potential additive effects of alternative phosphonate production, *P. ananatis* strain LMG 5342, which harbors HiVir, *Pgb,* and the *phn* phosphonate catabolism cluster, was used in a mutagenesis study. In *pgb* mutants, there was no difference in symptom development compared to backgrounds with mutagenized or intact HiVir, suggesting that pantaphos production is solely responsible for the disease phenotype in onion. Additionally, *phn* mutants with intact HiVir displayed more severe symptoms in onion than the wild-type strain,

suggesting phosphonate catabolism may interfere with full disease potential (Polidore et al. 2021).

Amazingly, HiVir has recently been found in the plasmids of other *Pantoea* species. A genomic analysis of *P. agglomerans* found a homologous cluster in two separate plasmid contexts. One location was on the conserved *P. agglomerans* plasmid (pAggl), and another on a mosaic cluster of plasmids shared among onion-isolated *P. agglomerans* (pOnion). The *P. agglomerans* cluster shared ~76% nucleotide identity with the chromosomal HiVir cluster of *P. ananatis* strain PNA97-1R (Shin et al. 2025).

Two recently sequenced genomes of *P. vagans* revealed one strain that harbored a gene cluster with ~87% identity to the HiVir cluster of *P. ananatis* strain PNA97-1R, again on a plasmid, but lacking *hvrK* entirely (549,416 bp in size). The sequenced strain containing HiVir was able to produce the hallmark necrotic lesions on onion, while the other, lacking HiVir, was not (Shin and Kvitko 2025).

In *P. stewartii* subsp. *indologens* the plasmid-borne HiVir operon shares even closer identity with *P. ananatis*, with 95% nucleotide identity between *P. stewartii* subsp. *indologenes* strain PNA 03-3 and *P. ananatis* strain PNA97-1R (Shin et al. 2025). Strains containing HiVir were able to induce necrosis in onion, but when HiVir *pepM* was mutated, lesions were abolished (Zhao et al. 2023).

Finally, *P. allii* strains carrying HiVir appear to be within a distinct lineage of *P. allii,* primarily isolated in the US. Yet again, HiVir presence was detected on a plasmid, this time with 94% similarity between *P. allii* strain 20TX0020 and PNA97-1R (Shin et al. 2025). As with *P.*

*ananatis* and *P. stewartii,* deletion of *pepM* within this cluster resulted in abolishment of necrosis in onion (Shin et al. 2026).

Despite pantaphos as the only known phosphonate that contributes to virulence within *P. ananatis,* another phosphonate molecule relevant to disease, named Halophos, was described in both *P. stewartii* subsp. *indologenes* and *P. allii* (Zhao et al. 2023). The pantaphos and Halophos biosynthetic gene clusters only share the *pepM* gene and the MFS transporter (35% and 32% similarity, respectively). For both species, deletion of *pepM* within the Halophos cluster eliminated symptom development (Zhao et al. 2023). Notably, the necrosis caused by pantaphos and Halophos is distinct. Pantaphos-containing strains produced a white clearing zone on red onion scales, while Halophos-containing strains produced sunken, yellow lesions (Zhao et al. 2023). Among genomes analyzed, no single strain harbored both pantaphos and Halophos biosynthetic gene clusters (Shin et al. 2026; Zhao et al. 2023). To date, Halophos has not been discovered in the genomes of *P. ananatis.*

For the HiVir operon in *P. ananatis*, the unique role of a SAM-dependent enzyme, and the requirement for SAM, could suggest the potential for metabolic cross-talk with quorum-sensing systems. SAM serves as a substrate for autoinducer biosynthesis in various bacterial systems (Schaefer et al. 1996; Schu et al. 2009; Wei et al. 2011). Competition for SAM by HvrF could theoretically link pantaphos production with quorum-sensing regulation. Other studies have investigated the role of Lux-type quorum-sensing systems in virulence of *P. ananatis* (Morohoshi et al. 2007; Sibanda et al. 2016). However, a direct link between quorum sensing and pantaphos has yet to be revealed and the possibility remains that no mechanistic connection exists between the pathways.

*Quorum sensing*

The quorum sensing system employed by *P. ananatis* is a *Lux*-type system mediated by N-acyl homoserine lactones (AHLs), with abundant and diverse AHL profiles reported across characterized strains.

This system consists of EanI, an AHL synthase, and EanR, the cognate receptor and transcriptional regulator, as described in *P. ananatis* strain Sk-1 (Morohoshi et al. 2007). In this initial characterization of *P. ananatis* quorum sensing, two main AHLs were identified as N-hexanoyl-L-homoserine lactone (C6-ASL) and N-(3-oxohexanoyl)-L-homoserine (3-oxo-C6-ASL).

Further characterization of this system in strain LMG2665 revealed that deletion of *eanI* abolished the ability to produce various short-chain AHLs (C4-C8) (Sibanda et al. 2016). A second *lux*-type system, RhlI/RhlR, was also detected, though the deletion of *rhlI* did not affect short chain AHL production (Sibanda et al. 2016). Production of long-chain AHLs remains a possibility. Importantly, both EanI/R and RhlI/R are required for full pathogenicity in onion, as *ean* and *rhl* knock-out mutations abolished symptom development in onion (Morohoshi et al. 2007; Sibanda et al. 2016). As expected, symptoms were restored in *eanI* mutants, but not *rhlI* mutants, through exogenous application of 3-oxo-C6-HSL (Morohoshi et al. 2007; Sibanda et al. 2016). One proposed mechanism by which virulence is inhibited is through reduced exopolysaccharide (EPS) production in mutants and impacted biofilm formation (Morohoshi et al. 2007).

Other publications have corroborated these results and provide evidence for additional AHL production. From strain CCT 6841, originally isolated from pineapple (Serrano 1928), C6-,

C7-, and C8-AHLs were detected (Pomini et al. 2006). In strain CWB304, isolated from the cabbage white butterfly larval midgut, 3-oxo-C6-, 3-oxo-C8-, C7-, and C8-AHLs were characterized (Borlee et al. 2008), and *P. ananatis* strain B9, isolated from marine snow, showed evidence of producing 3-oxo-C6-, C6-, C4-, C10-, C12-, and C14-AHLs (Jatt et al. 2015).

EanR acts as a transcriptional repressor, binding to promoter regions at a *lux*-box-like sequence termed the "*ean*-box" (Morohoshi et al. 2007). This sequence is present in the *eanR* promoter itself, creating a circuit that enables de-repression of *eanR* as part of the quorum sensing response (Morohoshi et al. 2007). In addition to self-regulation, *ean* mutants in strain LMG2665 displayed altered regulation of approximately 4.5% of the genome, impacting genes involved in redox sensing, metabolism, chemotaxis, membrane proteins, transport proteins, and cell wall synthesis (Sibanda et al. 2018).

*P. ananatis* quorum sensing is further regulated by a post-transcriptional network involving the RNA chaperone Hfq. Mutants of *hfq* displayed reduced *eanI* expression compared to wild-type and complemented strains (Choi et al. 2021), reduced motility, and were unable to develop disease symptoms in onion (Shin et al. 2019), consistent with previous results involving disrupted quorum sensing. Notably, *hfq* mutants showed differential regulation of two Hfq-dependent small RNAs (sRNAs) that are in close proximity to the *ean* locus. In wild-type, sRNAs pPAR237 and pPAR238 are abundant at low cell density and decrease at high cell density, but are completely absent in *hfq* mutants (Shin et al. 2019). *In silico* predictions suggest the possibility for interaction between the sRNAs and both DNA and mRNA sequences derived from the *ean* locus (Shin et al. 2019).

*Motility*

Like many pathogenic bacteria, motility is crucial for *P. ananatis* to locate attachment sites, disperse within host tissues, and establish successful infection. This bacterium utilizes multiple forms of motility that play complementary roles in infection of plant hosts.

Swimming motility is driven by peritrichous flagella. It's importance in virulence of *P. ananatis* was revealed through mutations in key flagellar genes, including the flagellar assembly gene *flgK* and the flagellar motor complex gene *motA.* Both mutations rendered strains non-pathogenic in onion, with mutants failing to induce disease symptoms (Weller-Stuart et al. 2017b).

In addition to swimming motility, *P. ananatis* uses twitching motility mediated by type IV pili (TFP). Key genes *pilA*, forming the structural subunit of TFP, and *pilT,* an ATPase that provides energy for use were mutated. Due to mutation, symptom development in onion was reduced compared to wild-type strains (Weller-Stuart et al. 2017b). Mutations of twitching motility likely disrupt bacterial adhesion to host surfaces, but unlike the absolute requirement observed for flagellar motility, the twitching motility system appears to have an additive effect on virulence (Weller-Stuart et al. 2017b).

*Secretion systems*

*P. ananatis* exhibits a secretion system profile that distinguishes it from many plant-pathogenic bacteria. It is widely reported to lack type II (T2SS), type III (T3SS), and type IV (T4SS) secretion systems, but usually possesses functional type I (T1SS), type V (T5SS), and type VI (T6SS) secretion systems (Coutinho and Venter 2009).

While noted for a lack of T3SS, the presence of *Pantoea* secretion island 2 (PSI-2) T3SS in *P. ananatis* strains 15320 and DAR76143 has been shown (Kirzinger et al. 2015). PSI-2 was described in *P. stewartii* and is homologous to the animal-specific *Salmonella* pathogenicity island 1 (SPI-1). In *P. stewartii*, PSI-2 enables its persistence within the gut of flea beetle insect vectors (Correa et al. 2012). The identification of this system in P. *ananatis* is particularly intriguing given the documented associations between *P. ananatis* and multiple insect hosts (Borlee et al. 2008; Dutta et al. 2016; Gitaitis et al. 2003; Krawczyk et al. 2021; Medrano and Bell 2015; Murrell et al. 2003; Watanabe et al. 1996; Watanabe and Sato 1999). In *P. ananatis,* PSI-2 may be involved in insect transmission or persistence, though this potential role has not been experimentally investigated. *P. stewartii* also contains *Pantoea* secretion island 1 (PSI-1), a Hrc 1 system, and *Pantoea* secretion island 3 (PSI-3; homologous to SPI-2 in *Salmonella*). PSI-1 is utilized for pathogenic interactions with plant hosts (Correa et al. 2012) but has not yet been identified in *P. ananatis.*

Compared to T3SS, more is known about the role of the T6SS in *P. ananatis.* Strains can harbor up to three distinct T6SS with varying functional capabilities and genomic distributions. T6SS-1 is a chromosomally encoded, universally present system across all *P. ananatis* strains, and contains all 13 core components for functionality. T6SS-2, located on the genus-wide LPP-1 plasmid, also contains all core components, but is restricted to a subset of genomes. Finally, T6SS-3 is present in all strains chromosomally, but lacks up to 11 of the core genes, rendering it unfunctional (Shyntum et al. 2014).

When tested for involvement in pathogenicity, T6SS-1 *P. ananatis* mutants were unable to cause disease in onion, while wild-type was virulent (Shyntum et al. 2015; Zhao et al. 2024), highlighting its role in pathogenicity. T6SS-1 mutants also performed poorly in bacterial

competition assays against other Gram-negative bacteria compared to wild-type (Zhao et al. 2024), indicating dual roles in plant pathogenicity and bacterial competition. TseG has been identified as a key effector protein of this secretion system. It requires the chaperone protein TecG for delivery, and is neutralized by the immunity protein TsiG (Zhao et al. 2024). Similar to T6SS-1 mutants, *tseG* mutants displayed reduced lesion development on onion, as well as potato and maize (Zhao et al. 2024). The toxicity of TseG was demonstrated by its ability to slow *E. coli* growth when cloned and heterologously expressed (Zhao et al. 2024).

T6SS-2 does not have a synergistic effect with T6SS-1 and T6SS-2 mutants did not impact bacterial competition (Zhao et al. 2024). In contrast, T6SS-3 had no detectable impact on pathogenicity or bacterial competition, consistent with its incomplete gene repertoire and presumed non-functional status (Shyntum et al. 2015; Zhao et al. 2024)

Together, these findings establish T6SS as important for host interactions and bacterial competition for *P. ananatis*, but also point to the potential involvement of T3SS within the *P. ananatis* population, perhaps involving insect interactions, although more experimentation is needed.

*Plasmids*

The genus *Pantoea* shares the large *Pantoea* plasmid (LPP-1) that appears to have been derived from a common ancestor (De Maayer et al. 2012; Shetty et al. 2024). The overall profile of LPP-1 can be differentiated into three distinct groups (I-III). *P. ananatis* harbors the group II LPP-1 plasmid, along with *P. stewartii,* while groups I and III are distributed among other members of the genus (De Maayer et al. 2012; Shetty et al. 2024). Despite all *P. ananatis* strains sharing group II LPP-1, large amounts of genetic diversity within the plasmid exist between

strains, as a majority of the plasmid coding sequence (CDS) content is described as flexible (De Maayer et al. 2012). There are several key features that can be found in some group II LPP-1 plasmids: glucoamylase, allowing for glucose release from starch; pyrimidine catabolism as an alternate nitrogen source; tyrosine transport for amino acid utilization; type 6 secretion systems; 2,3-butanediol biosynthesis, which can induce plant systemic resistance; and flagellin and fimbrial system genes (De Maayer et al. 2012). The mentioned components have the potential to play vital roles in how a strain of *P. ananatis* interacts with its host or environment.

To highlight the plasmid's role in pathogenicity, a plasmid elimination strategy was used to knock out the group II LPP-1 plasmid from maize-pathogenic *P. ananatis* strain DZ-12 (plasmid pDZ-12). When eliminated, mutant DZ-12 strains lacked full pathogenicity in maize plants, had reduced biofilm formation capability, and disrupted carotenoid pigment production (Zhao et al. 2021).

LPP-1 represents a well-understood plasmid for the species, but strains can harbor many other unique plasmids that are not as widely distributed across the species, complicating the full understanding of the role that plasmids play in disease interactions (Shetty et al. 2024).

*Enzymes*

Many plant pathogenic bacteria use enzymes to degrade plant polymers as they are useful tools for infiltrating plants by breaking down barriers to entry and for acquiring nutrients (Charkowski 2018; Kubicek et al. 2014).

In *P. ananatis,* little functional experimentation has been done to verify the activity and mechanism of such enzymes, although a novel carbohydrate esterase that contributed to lignin degradation was discovered in strain Sd-1 (Yao et al. 2020). The secretome of this strain

displayed enzymatic activities characteristic of endoglucanases, exoglucanases, and β-glucosidase, and displayed high levels of saccharification of rice straw media, indicating lignocellulose degradation activity (Ma et al. 2016). In genomic analyses, orthologs of plant carbohydrate degradation proteins endo-1,4-β-xylanase, polygalacturonase, pectin acetylesterase, and cellulase were identified, though activities were not tested (De Maayer et al. 2014).

*Surviving host defenses*

Because of the vast host range of *P. ananatis*, it must be able to equip itself with mechanisms to tolerate plant defenses. To date, one such system has been identified in association with *P. ananatis* infection of onion, where a classic arms race has emerged (Stice et al. 2020). This chemical battle, which begins when *P. ananatis* produces pantaphos, results in damaged host cells. The wounded onion mounts a counterattack by producing thiosulfinates, reactive organosulfur compounds generated in response to damage. These chemicals represent a rapid, potent chemical defense mechanism where enzymes stored in separate subcellular compartments are released, allowing them to mix and catalyze the formation of the thiosulfinates (Stice et al. 2020).

One of the most studied thiosulfinates is allicin in garlic. It reacts with cellular thiols and results in protein modifications that lead to the deactivation of enzymes and aggregation of proteins. Additionally, allicin reacts with and depletes the cellular store of reduced glutathione, a critical component of antioxidant defenses (Stice et al. 2020). Onion extract contains similar thiosulfinates that restrict *Pantoea* growth, comparable to growth reduction when exposed to purified allicin (Stice et al. 2020).

To combat this chemical defense produced by onion, *P. ananatis* can harbor a plasmid-borne gene cluster, termed *alt* (for allicin tolerance). This cluster consists of eleven genes that are thought to enable *P. ananatis* to protect reduced glutathione from thiol stress. Each *alt* gene has additive protection as multiple genes within the cluster independently confer partial resistance phenotypes (Stice et al. 2020). Importantly, strains lacking the *alt* cluster can still trigger localized tissue necrosis in onion as long as they possess the HiVir operon, but the *alt* genes enhance pathogen performance within host tissue (Stice et al. 2020)

Recently, AltR, a TetR-family transcriptional repressor, has been revealed as the key regulatory component for the expression of the *alt* cluster (Jan et al. 2025). Under non-stress conditions, AltR represses the *alt* operon, binding to the "*alt* box", a sequence of inverted repeats in the *alt* promoter. Upon exposure to thiosulfinates, the *alt* promoter is de-repressed from AltR and activation of *alt* gene expression occurs. This regulatory mechanism was highly specific for thiosulfinates, not responding to general oxidative stress or other disulfides, indicating evolution to specifically detect defenses deployed by allium species (Jan et al. 2025).

The mechanism of AltR is dependent on the Cys100 residue within its protein sequence. Substitution of this residue with serine abolished responsive derepression of *alt*, implying that thiosulfinate detection involves chemical modification of this cysteine residue (Jan et al. 2025).

**Knowledge gaps in the rice pathosystem**

Despite extensive work in the *P. ananatis* – onion pathosystem, the molecular determinants of virulence in rice remain largely unresolved. Much of what is currently inferred for rice is extrapolated from onion, yet several lines of evidence suggest that pathogenicity in rice may follow a fundamentally different pattern.

Core systems such as quorum-sensing networks, extracellular enzyme production, motility systems, LPP-1 plasmid-encoded factors, and T6SS are broadly conserved across *P. ananatis* strains, and are therefore plausible contributors to host colonization in rice. However, their roles in this pathosystem remain experimentally untested, and it is unclear whether they function primarily in host interaction, microbial competition, or environmental persistence in the rice phyllosphere.

Intriguingly, virulence traits defined in onion have not been definitively linked to rice. Pantaphos production, mediated by the HiVir operon, is a primary determinant of virulence and necrotic symptom development in onion and other hosts, yet its role in rice remains ambiguous. Similarly, the role of the *alt* gene cluster, which confers tolerance to thiosulfonates in allium species, is unknown in rice.

Emerging phylogenetic analyses point towards a model in which *P. ananatis* lineages differ in their gene content and possibly in their strategies of host association. Genomic analyses suggest the presence of at least two major clades within the species, with one lineage showing strong association to rice and reduced genomic variability. This pattern is consistent with ecological specialization and suggests the rice-associated strains may rely on distinct, currently unidentified factors for successful colonization and persistence.

A key unresolved question, therefore, is whether rice pathogenicity is driven primarily by classical virulence determinants that induce host damage, or by traits that enable efficient colonization of host tissues with limited host disruption. In this study, I attempt to resolve these questions by integrating population genomics with functional assays in the rice system.

Placing *P. ananatis* within the broader context of the rice phytobiome may be critical for understanding its emergence as a pathogen. Given its demonstrated capacity for epiphytic, endophytic, and beneficial interactions in other systems, it is plausible that disease in rice represents a shift along a continuum of plant association rather than a strictly pathogenic state. Unravelling these roles will be particularly important for predicting disease risk and for developing management strategies.

## REFERENCES


Agarwal, G., Choudhary, D., Stice, S. P., Myers, B. K., Gitaitis, R. D., Venter, S. N., Kvitko, B. H., and Dutta, B. 2021. Pan-genome-wide analysis of *Pantoea ananatis* identified genes linked to pathogenicity in onion. Front. Microbiol. 12:684756.

Alhusays, A., Galvin, C., Torres, M., Senger, M., Fitzpatrick, E., Gonzalez-Hernandez, J. L., Glover, K., Solanki, S., and Ameen, G. 2024. First report of *Pantoea ananatis* causing leaf streak disease on wheat (*Triticum aestivum*) in the United States of America. Plant Dis. 108:2913.

Arias, R., Power, I., Culbreath, A., Sobolev, V., and Lamb, M. 2013. First report of *Pantoea ananatis* (syn. *Erwinia uredovora*) being associated with peanut rust in Georgia. Plant Health Prog. 14:48.

Asselin, J. A. E., Bonasera, J. M., and Beer, S. V. 2018. Center rot of onion (*Allium cepa*) caused by *Pantoea ananatis* requires *pepM*, a predicted phosphonate-related gene. Mol. Plant-Microbe Interact. 31:1291–1300.

Azad, H., Holmes, G., and Cooksey, D. 2000. A new leaf blotch disease of sudangrass caused by *Pantoea ananas* and *Pantoea stewartii*. Plant Dis. 84:973–979.

Azizi, M. M. F., Ismail, S. I., Ina-Salwany, M. Y., Hata, E. M., and Zulperi, D. 2020. The emergence of *Pantoea* species as a future threat to global rice production. J. Plant Prot. Res.:327–335.

Bing, X.-L., Wan, Y.-Y., Liu, H.-H., Ji, R., Zhao, D.-S., Niu, Y.-D., Li, T.-P., and Hong, X.-Y. 2022. Characterization of *Pantoea ananatis* from rice planthoppers reveals a clade of rice-associated *P. ananatis* undergoing genome reduction. Microb. Genom. 8:000907.

Borlee, B. R., Geske, G. D., Robinson, C. J., Blackwell, H. E., and Handelsman, J. 2008. Quorum-sensing signals in the microbial community of the cabbage white butterfly larval midgut. ISME J. 2:1101–1111.

Bowman, E., McQueney, M., Barry, R. J., and Dunaway-Mariano, D. 1988. Catalysis and thermodynamics of the phosphoenolpyruvate/phosphonopyruvate rearrangement. Entry into the phosphonate class of naturally occurring organophosphorus compounds. J. Am. Chem. Soc. 110:5575–5576.

Bragard, C., Baptista, P., Chatzivassiliou, E., Di Serio, F., Gonthier, P., Jaques Miret, J. A., Justesen, A. F., MacLeod, A., and Magnusson, C. S. 2023. Pest categorisation of *Pantoea ananatis*. EFSA J. 21:e07849.

Bruno, J., Barphagha, I., Ontoy, J., Dalla Lana, F., and Ham, J. H. 2025. First report of *Pantoea ananatis* causing bacterial leaf and panicle blight of rice in Louisiana, USA. Plant Dis. 109:932.

Charkowski, A. O. 2018. The changing face of bacterial soft-rot diseases. Annu. Rev. Phytopathol. 56:269–288.

Choi, O., Kang, B., Lee, Y., Lee, Y., and Kim, J. 2021. *Pantoea ananatis* carotenoid production confers toxoflavin tolerance and is regulated by Hfq-controlled quorum sensing. Microbiologyopen 10:e1143.

Correa, V. R., Majerczak, D. R., Ammar, E.-D., Merighi, M., Pratt, R. C., Hogenhout, S. A., Coplin, D. L., and Redinbaugh, M. G. 2012. The bacterium *Pantoea stewartii* uses two different type III secretion systems to colonize its plant host and insect vector. Appl. Environ. Microbiol. 78:6327–6336.

Coutinho, T. A., and Venter, S. N. 2009. *Pantoea ananatis*: an unconventional plant pathogen. Mol. Plant Pathol. 10:325–335.

Crosby, K. C., Rojas, M., Sharma, P., Johnson, M. A., Mazloom, R., Kvitko, B. H., Smits, T. H., Venter, S. N., Coutinho, T. A., and Heath, L. S. 2023. Genomic delineation and description of species and within-species lineages in the genus *Pantoea*. Front. Microbiol. 14:1254999.

De Maayer, P., Chan, W.-Y., Blom, J., Venter, S. N., Duffy, B., Smits, T. H., and Coutinho, T. A. 2012. The large universal *Pantoea* plasmid LPP-1 plays a major role in biological and ecological diversification. BMC Genom. 13:625.

De Maayer, P., Chan, W. Y., Rubagotti, E., Venter, S. N., Toth, I. K., Birch, P. R., and Coutinho, T. A. 2014. Analysis of the *Pantoea ananatis* pan-genome reveals factors underlying its ability to colonize and interact with plant, insect and vertebrate hosts. BMC Genom. 15:1–14.

De Maayer, P., Aliyu, H., Vikram, S., Blom, J., Duffy, B., Cowan, D. A., Smits, T. H., Venter, S. N., and Coutinho, T. A. 2017. Phylogenomic, pan-genomic, pathogenomic and evolutionary genomic insights into the agronomically relevant enterobacteria *Pantoea ananatis* and *Pantoea stewartii*. Front. Microbiol. 8:1755.

de Paula, S., Belmar, S., Giebler, M., Ferreira, A. C., Ronning, B., Jia, Y., Pedrozo, R., Leach, J. E., Luna, E., and Nicolli, C. 2026. Unraveling the Dynamics of *Pantoea ananatis*: Isolation and Plant Responses. Phytopathology.

Duchateau, S., Borrego, C., Verdelet, S., Dorey, S., Aziz, A., Dhondt-Cordelier, S., Gauthier, C., Déziel, É., Cordelier, S., and Crouzet, J. 2025. Growth-promoting and biocontrol features of *Pantoea ananatis* BRT175 in tomato. Biol. Control:105949.

Dutta, B., Gitaitis, R., Barman, A., Avci, U., Marasigan, K., and Srinivasan, R. 2016. Interactions Between *Frankliniella fusca* and *Pantoea ananatis* in the Center Rot Epidemic of Onion (*Allium cepa*). Phytopathology 106:956–962.

Gasser, F., Cardinale, M., Schildberger, B., and Berg, G. 2012. Biocontrol of *Botrytis cinerea* by successful introduction of *Pantoea ananatis* in the grapevine phyllosphere. Int. J. Wine Res.:53–63.

Gitaitis, R., and Gay, J. 1997. First report of a leaf blight, seed stalk rot, and bulb decay of onion by *Pantoea ananas* in Georgia. Plant Dis. 81:1096–1096.

Gitaitis, R., Walcott, R., Culpepper, S., Sanders, H., Zolobowska, L., and Langston, D. 2002. Recovery of *Pantoea ananatis*, causal agent of center rot of onion, from weeds and crops in Georgia, USA. Crop Prot. 21:983–989.

Gitaitis, R. D., Walcott, R. R., Wells, M. L., Perez, J. C. D., and Sanders, F. H. 2003. Transmission of *Pantoea ananatis*, Causal Agent of Center Rot of Onion, by Tobacco Thrips, *Frankliniella fusca*. Plant Dis. 87:675–678.

Hidaka, T., Mori, M., Imai, S., Hara, O., Nagaoka, K., and Seto, H. 1989. Studies on the biosynthesis of bialaphos (SF-1293). 9. Biochemical mechanism of C-P bond formation in bialaphos: discovery of phosphoenolpyruvate phosphomutase which catalyzes the formation of phosphonopyruvate from phosphoenolpyruvate. J. Antibiot. 42:491–494.

Jan, H.-H., Kong, F., MacLellan, M. P., Yang, L., Dutta, B., and Kvitko, B. H. 2025. The AltR transcription factor responds to plant thiosulfinates to regulate gene expression in a bacterial pathogen of onion. bioRxiv:2025.2011. 2019.689302.

Jatt, A. N., Tang, K., Liu, J., Zhang, Z., and Xiao-Hua, Z. 2015. Quorum sensing in marine snow and its possible influence on production of extracellular hydrolytic enzymes in marine snow bacterium *Pantoea ananatis* B9. FEMS Microbiol. Ecol. 91:1–13.

Ju, K.-S., Doroghazi, J. R., and Metcalf, W. W. 2014. Genomics-enabled discovery of phosphonate natural products and their biosynthetic pathways. Journal of Industrial Microbiology and Biotechnology 41:345–356.

Kang, S. H., Cho, H., Cheong, H., Ryu, C., Kim, J. F., and Park, S. 2007. Two bacterial entophytes eliciting both plant growth promotion and plant defense on pepper (*Capsicum annuum* L.). J. Microbiol. Biotechnol. 17:96.

Khanal, S., Zhou, X.-G., and Jia, Y. Unpublished. First Report of Rice Bacterial Leaf Blight Caused by *Pantoea ananatis* in Texas, USA.

Kirzinger, M. W., Butz, C. J., and Stavrinides, J. 2015. Inheritance of *Pantoea* type III secretion systems through both vertical and horizontal transfer. Mol. Genet. Genomics 290:2075–2088.

Krawczyk, K., Foryś, J., Nakonieczny, M., Tarnawska, M., and Bereś, P. K. 2021. Transmission of *Pantoea ananatis*, the causal agent of leaf spot disease of maize (*Zea mays*), by western corn rootworm (*Diabrotica virgifera virgifera* LeConte). Crop Prot. 141:105431.

Kubicek, C. P., Starr, T. L., and Glass, N. L. 2014. Plant cell wall–degrading enzymes and their secretion in plant-pathogenic fungi. Annu. Rev. Phytopathol. 52:427–451.

LaGier, M. J., McDaniel, M., Ragner, A., and Castillo, A. 2022. Identification and characterization of a potential antibiotic producing strain of *Pantoea ananatis*. J. Genom. 10:26.

Lee, J., Jung, W.-K., Ahsan, S., Jung, H.-Y., and Choi, H. W. 2024. Identification of *Pantoea ananatis* strain BCA19 as a potential biological control agent against *Erwinia amylovora*. Front. Microbiol. 15:1493430.

Lu, L., Chang, M., Han, X., Wang, Q., Wang, J., Yang, H., Guan, Q., and Dai, S. 2021. Beneficial effects of endophytic *Pantoea ananatis* with ability to promote rice growth under saline stress. J. Appl. Microbiol. 131:1919–1931.

Luhung, I., Junqueira, A., Uchida, A., Purbojati, R., Houghton, J., Chénard, C., Wong, A., Clare, M., Kushwaha, K., and Panicker, D. 2018. Genome sequence of *Pantoea ananatis* SGAir0210, isolated from outdoor air in Singapore. Genome Announc.:e00643–00618.

Luna, E., Lang, J., McClung, A., Wamishe, Y., Jia, Y., and Leach, J. E. 2023. First report of rice bacterial leaf blight disease caused by *Pantoea ananatis* in the United States. Plant Dis. 107:2214.

Ma, J., Zhang, K., Liao, H., Hector, S. B., Shi, X., Li, J., Liu, B., Xu, T., Tong, C., and Liu, X. 2016. Genomic and secretomic insight into lignocellulolytic system of an endophytic bacterium *Pantoea ananatis* Sd-1. Biotechnol. Biofuels Bioprod. 9:25.

Medrano, E. G., and Bell, A. A. 2015. Genome sequence of *Pantoea ananatis* strain CFH 7-1, which is associated with a vector-borne cotton fruit disease. Genome Announc. 3:10.1128/genomea. 01029–01015.

Megías, E., Megías, M., Ollero, F. J., and Hungria, M. 2016. Draft genome sequence of *Pantoea ananatis* strain AMG521, a rice plant growth-promoting bacterial endophyte isolated from the Guadalquivir marshes in southern Spain. Genome Announc. 4:10–1128.

Morohoshi, T., Nakamura, Y., Yamazaki, G., Ishida, A., Kato, N., and Ikeda, T. 2007. The plant pathogen *Pantoea ananatis* produces N-acylhomoserine lactone and causes center rot disease of onion by quorum sensing. J. Bacteriol. 189:8333–8338.

Murrell, A., Dobson, S. J., Yang, X., Lacey, E., and Barker, S. C. 2003. A survey of bacterial diversity in ticks, lice and fleas from Australia. Parasitol. Res. 89:326–334.

Obasa, K., Coker, D., and Santiago-Gonzalez, J. 2024. Late-season decline, a bacterial disease of corn caused by *Pantoea ananatis*, identified in sorghum. Plant Health Prog. 25:348–352.
Obasa, K., Kolomiets, M., Reed, B., Coker, D., Bell, J., and Heflin, K. 2023. Late-season decline: A new bacterial disease of corn identified in the Texas panhandle. Plant Health Prog. 24:198–206.
Pileggi, M., Pileggi, S. A., Olchanheski, L. R., da Silva, P. A., Munoz Gonzalez, A. M., Koskinen, W. C., Barber, B., and Sadowsky, M. J. 2012. Isolation of mesotrione-degrading bacteria from aquatic environments in Brazil. Chemosphere 86:1127–1132.
Polidore, A. L., Caserio, A. D., Zhu, L., and Metcalf, W. W. 2024. Complete biochemical characterization of pantaphos biosynthesis highlights an unusual role for a SAM-dependent methyltransferase. Angew. Chem. Int. Ed. 63:e202317262.
Polidore, A. L. A., Furiassi, L., Hergenrother, P. J., and Metcalf, W. W. 2021. A phosphonate natural product made by *Pantoea ananatis* is necessary and sufficient for the hallmark lesions of onion center rot. Mbio 12:10.1128.
Pomini, A. M., Araújo, W. L., and Marsaioli, A. J. 2006. Structural elucidation and biological activity of acyl-homoserine lactones from the phytopathogen *Pantoea ananatis* Serrano 1928. J. Chem. Ecol. 32:1769–1778.
Rauch, M. E., Graef, H. W., Rozenzhak, S. M., Jones, S. E., Bleckmann, C. A., Kruger, R. L., Naik, R. R., and Stone, M. O. 2006. Characterization of microbial contamination in United States Air Force aviation fuel tanks. J. Ind. Microbiol. Biotechnol. 33:29–36.
Schaefer, A. L., Val, D. L., Hanzelka, B. L., Cronan Jr, J. E., and Greenberg, E. P. 1996. Generation of cell-to-cell signals in quorum sensing: acyl homoserine lactone synthase activity of a purified *Vibrio fischeri* LuxI protein. Proc. Natl. Acad. Sci. USA 93:9505–9509.
Schu, D. J., Carlier, A. L., Jamison, K. P., von Bodman, S., and Stevens, A. M. 2009. Structure/function analysis of the Pantoea stewartii quorum-sensing regulator EsaR as an activator of transcription. J. Bacteriol. 191:7402–7409.
Seidel, H. M., Freeman, S., Seto, H., and Knowles, J. R. 1988. Phosphonate biosynthesis: isolation of the enzyme responsible for the formation of a carbon–phosphorus bond. Nature 335:457–458.
Serrano, F. 1928. Bacterial fruitlet brown-rot of pineapple in the Philippines. The Philippine Journal of Science 36:271–305.
Sheibani-Tezerji, R., Naveed, M., Jehl, M.-A., Sessitsch, A., Rattei, T., and Mitter, B. 2015. The genomes of closely related *Pantoea ananatis* maize seed endophytes having different effects on the host plant differ in secretion system genes and mobile genetic elements. Front. Microbiol. 6:440.
Shetty, S., Kamble, A., and Singh, H. 2024. Insights into the potential role of plasmids in the versatility of the genus *Pantoea*. Mol. Biotechnol. 66:3398–3414.
Shin, G. Y., and Kvitko, B. H. 2025. Complete genome sequences of *Pantoea vagans* strains GM1 and GM2, isolated from the leaves of garlic mustard. Microbiol. Resour. Announc. 14:e00943–00924.
Shin, G. Y., Dutta, B., and Kvitko, B. 2023. The genetic requirements for HiVir-mediated onion necrosis by *Pantoea ananatis*, a necrotrophic plant pathogen. Mol. Plant-Microbe Interact. 36:381–391.
Shin, G. Y., Schachterle, J. K., Shyntum, D. Y., Moleleki, L. N., Coutinho, T. A., and Sundin, G. W. 2019. Functional characterization of a global virulence regulator Hfq and

identification of Hfq-dependent sRNAs in the plant pathogen *Pantoea ananatis*. Front. Microbiol. 10:2075.
Shin, G. Y., Asselin, J. A., Smith, A., Aegerter, B., Coutinho, T., Zhao, M., Dutta, B., Mazzone, J., Neupane, R., and Gugino, B. 2025. Plasmids encode and can mobilize onion pathogenicity in *Pantoea agglomerans*. ISME J. 19:wraf019.
Shin, G. Y., De Armas, S., Galván, G. A., Siri, M. I., Rojas, M., Vinatzer, B. A., Asselin, J. A. E., Stodghill, P., Zhao, M., and Dutta, B. 2026. Comparative genomics of *Pantoea allii* lineages and distribution of ecologically relevant traits. Microb. Genom. 12:001624.
Shyntum, D. Y., Venter, S. N., Moleleki, L. N., Toth, I., and Coutinho, T. A. 2014. Comparative genomics of type VI secretion systems in strains of *Pantoea ananatis* from different environments. BMC Genom. 15:163.
Shyntum, D. Y., Theron, J., Venter, S. N., Moleleki, L. N., Toth, I. K., and Coutinho, T. A. 2015. *Pantoea ananatis* utilizes a type VI secretion system for pathogenesis and bacterial competition. Mol. Plant-Microbe Interact. 28:420–431.
Sibanda, S., Theron, J., Shyntum, D. Y., Moleleki, L. N., and Coutinho, T. A. 2016. Characterization of two LuxI/R homologs in *Pantoea ananatis* LMG 2665T. Can. J. Microbiol. 62:893–903.
Sibanda, S., Kwenda, S., Tanui, C. K., Shyntum, D. Y., Coutinho, T. A., and Moleleki, L. N. 2018. Transcriptome profiling reveals the EanI/R quorum sensing regulon in *Pantoea ananatis* LMG 2665T. Genes 9:148.
Stice, S. P., Thao, K. K., Khang, C. H., Baltrus, D. A., Dutta, B., and Kvitko, B. H. 2020. Thiosulfinate tolerance is a virulence strategy of an atypical bacterial pathogen of onion. Curr. Biol. 30:3130–3140.
Thomas, P., Kumari, S., Swarna, G. K., and Gowda, T. 2007. Papaya shoot tip associated endophytic bacteria isolated from in vitro cultures and host–endophyte interaction in vitro and in vivo. Can. J. Microbiol. 53:380–390.
Tian, Y., Lei, W., Zhang, J., Shen, Y., Lu, J., Ijaz, M., Alrafaie, A., Ahmed, T., Yan, C., and Li, B. 2026. Mechanism of *Pantoea ananatis* in the biocontrol of rice bacterial leaf blight. Front. Microbiol. 17:1722838.
Wang, D. R., Jamshidi, S., Han, R., Edwards, J. D., McClung, A. M., and McCouch, S. R. 2024. Positive effects of public breeding on US rice yields under future climate scenarios. Proc. Natl. Acad. Sci. USA 121:e2309969121.
Watanabe, K., and Sato, M. 1999. Gut colonization by an ice nucleation active bacterium, *Erwinia* (*Pantoea)* ananas reduces the cold hardiness of mulberry pyralid larvae. Cryobiology 38:281–289.
Watanabe, K., Kawakita, H., and Sato, M. 1996. Epiphytic bacterium, *Erwinia ananas*, commonly isolated from rice plants and brown planthoppers (*Nilaparvata lugens*) in hopperburn patches. Appl. Entomol. Zool. 31:459–462.
Wei, Y., Perez, L. J., Ng, W.-L., Semmelhack, M. F., and Bassler, B. L. 2011. Mechanism of *Vibrio cholerae* autoinducer-1 biosynthesis. ACS Chem. Biol. 6:356–365.
Weller-Stuart, T., De Maayer, P., and Coutinho, T. 2017a. *Pantoea ananatis*: genomic insights into a versatile pathogen. Mol. Plant Pathol. 18:1191–1198.
Weller-Stuart, T., Toth, I., De Maayer, P., and Coutinho, T. 2017b. Swimming and twitching motility are essential for attachment and virulence of *Pantoea ananatis* in onion seedlings. Mol. Plant Pathol. 18:734–745.

Wells, J., Sheng, W., Ceponis, M., and Chen, T. 1987. Isolation and characterization of strains of *Erwinia ananas* from honeydew melons. Phytopathology 77:511–514.

Yao, Q., Huang, M., Bu, Z., Zeng, J., Wang, X., Liu, Z., Ma, J., Zhang, K., Liu, X., and Zhu, Y. 2020. Identification and characterization of a novel bacterial carbohydrate esterase from the bacterium *Pantoea ananatis* Sd-1 with potential for degradation of lignocellulose and pesticides. Biotechnol. Lett. 42:1479–1488.

Zhao, M., Shin, G. Y., Stice, S., Bown, J. L., Coutinho, T., Metcalf, W. W., Gitaitis, R., Kvitko, B., and Dutta, B. 2023. A novel biosynthetic gene cluster across the *Pantoea* species complex is important for pathogenicity in onion. Mol. Plant-Microbe Interact. 36:176–188.

Zhao, X., Gao, L., Huang, H., Zhao, Y., Hanif, A., Wu, H., Gu, Q., Wu, L., and Gao, X. 2021. Exploring the pathogenic function of *Pantoea ananatis* endogenous plasmid by an efficient and simple plasmid elimination strategy. Microbiol. Res. 246:126710.

Zhao, X., Gao, L., Ali, Q., Yu, C., Yuan, B., Huang, H., Long, J., Gu, Q., Wu, H., and Gao, X. 2024. A type VI secretion system effector TseG of *Pantoea ananatis* is involved in virulence and antibacterial activity. Mol. Plant Pathol. 25:e13442.

# CHAPTER 2: DISTINCT LINEAGES OF *PANTOEA ANANATIS* ASSOCIATED WITH RICE DIFFER IN TOXIN BIOSYNTHESIS GENE CONTENT AND HOST SPECIALIZATION[1]

## Introduction

*Pantoea ananatis* is a Gram-negative, yellow-pigmented bacterium in the family *Erwiniaceae* that occupies a wide range of ecological niches (Coutinho and Venter 2009; Weller-Stuart et al. 2017a; Zhao et al. 2021); the species has been isolated from diverse environmental sources, including soil, water, air, aviation fuel tanks, as well as from plant, insect, and even human hosts (De Maayer et al. 2014; LaGier et al. 2022; Luhung et al. 2018; Morohoshi et al. 2007; Rauch et al. 2006). In agricultural systems, *P. ananatis* frequently occurs as both an epiphyte living on leaf surfaces (Gitaitis et al. 2002; Watanabe et al. 1996) and as an endophyte within plant tissues (Mano et al. 2006; Okunishi et al. 2005; Sheibani-Tezerji et al. 2015). Such occurrences are frequently asymptomatic, and several strains of *P. ananatis* have been reported to exhibit plant growth promoting properties (Kim et al. 2012; Megías et al. 2016). Despite this,

---

[1] Published in *Phytopathology* June 17, 2026. DOI: https://doi.org/10.1094/PHYTO-04-26-0138-R

Authors: Mitchell Giebler[1], Emily Luna[1], Camila Nicolli[2,3], Federico Martin[1], Rodrigo Pedrozo[4], Prasanna Joglekar[5], Alejandra I. Huerta[5], Yulin Jia[6], Jan E. Leach[1]

[1] Department of Agricultural Biology, Colorado State University, Ft. Collins, CO 80523-1177, U.S.A.; [2] Department of Entomology and Plant Pathology, Division of Agriculture, Rice Research & Extension Center, University of Arkansas, Stuttgart, AR 72160, U.S.A.; [3] Department of Botany and Plant Pathology, Purdue University, West Lafayette, IN 47907, U.S.A.; [4] ORISE Fellow, USDA ARS Dale Bumpers National Rice Research Center, Stuttgart, AR 72160, U.S.A.; [5] Department of Entomology and Plant Pathology, North Carolina State University, Raleigh, NC 27606, U.S.A.; [6] USDA ARS Dale Bumpers National Rice Research Center, Stuttgart, AR 72160, U.S.A.

the species is increasingly recognized as an opportunistic pathogen capable of causing disease on a wide range of crop hosts (Azizi et al. 2020).

The ecological versatility of *P. ananatis* is thought to stem, in part, from extensive genomic plasticity. Comparative genomic analyses have shown that the species possesses an open pan-genome comprising a conserved core genome and a large accessory genome that continues to expand as new strains are sequenced (Agarwal et al. 2021; Weller-Stuart et al. 2017a). This expansive accessory genome likely plays a key role in facilitating adaptation to diverse ecological niches and host environments (Weller-Stuart et al. 2017a). Consistent with this hypothesis, *P. ananatis* has been reported to cause disease in a wide range of monocots and dicots (Chathalingath and Gunasekar 2023; Cota et al. 2010; Coutinho et al. 2002; Das et al. 2020; Gao et al. 2024; Gitaitis and Gay 1997; Goszczynska et al. 2007; Gutiérrez-Barranquero et al. 2019; Kido et al. 2008; Krawczyk et al. 2020; Lao et al. 2023; Liao et al. 2016; Mondal et al. 2011; Serrano 1928; Wang et al. 2019; Yuan et al. 2023; Zhang et al. 2019). Disease symptoms typically manifest as blight-like lesions on leaves, stems, or modified stems such as onion bulbs, (Coutinho and Venter 2009; Luna et al. 2023; Mondal et al. 2011), although infections of reproductive tissues have also been reported in monocots (Azad et al. 2000; Bruno et al. 2025; Goszczynska et al. 2007; Yan et al. 2010).

The global relevance of plant-pathogenic *P. ananatis* is rising, marked by a surge in disease reports across a range of geographic regions (Fig. 1, Table S1). In the USA, despite decades of recognition as a pathogen to multiple crops (Alhusays et al. 2024; Gitaitis and Gay 1997; Obasa et al. 2024; Obasa et al. 2023; Schwartz and Otto 2000), *P. ananatis* has only recently been reported, with increasing frequency, in rice (Bruno et al. 2025; de Paula et al. 2026; Luna et al. 2023). This emergence raises concerns, considering the economic importance

of rice in the USA, where the crop contributes approximately $2.6 billion annually to the agricultural economy, and nearly 45% of the rice produced is exported to international markets (Wang et al. 2024).

Effective management of this emerging threat is hindered by a limited understanding of the molecular mechanisms underlying its pathogenicity in rice. Remarkably, *P. ananatis* generally lacks several canonical virulence systems that define Gram-negative plant pathogens, including the Type II (T2SS) and Type III (T3SS) secretion systems that are otherwise found in phytopathogenic genera such as *Pseudomonas* and *Xanthomonas* (Stice et al. 2020). Instead, pathogenicity of *P. ananatis* in several plant hosts has been linked to alternative mechanisms. One of the best characterized virulence determinants for this pathogen is the HiVir gene cluster, which encodes the biosynthesis of the phosphonate phytotoxin pantaphos (2-[hydroxy(phosphono)methyl]maleate) (Asselin et al. 2018; Polidore et al. 2024; Polidore et al. 2021). This molecule is associated with host tissue damage and symptom development in susceptible plants (Asselin et al. 2018; Shin et al. 2023). Additional pathogenicity factors in certain hosts include quorum sensing systems, motility mechanisms, and Type VI secretion systems involved in both interbacterial competition and host interactions (Morohoshi et al. 2007; Sibanda et al. 2016; Stice et al. 2020; Weller-Stuart et al. 2017b; Zhao et al. 2024). In onion and other Allium hosts, tolerance of host-derived thiosulfinate chemical defenses has been linked to the *alt* (allicin tolerance) gene cluster (Stice et al. 2020). However, it remains unclear which, if any, of these mechanisms are relevant during rice infection.

The rice pathosystem appears to be unique among those involving *P. ananatis.* Recent phylogenomic analyses suggest that *P. ananatis* may be structured into two distinct evolutionary lineages, including groups that differ in genome size, gene content, and host associations (Bing et

al. 2022;  De Maayer et al. 2017). One evolutionary lineage is characterized by genome reduction and includes rice-isolated strains, with a notable absence of strains recovered from other hosts. The practical consequences of evolutionary divergence among these populations remain unclear, raising the possibility that distinct *P. ananatis* lineages may employ different infection strategies in rice, potentially complicating the study of disease development.

In this study, we investigated the population structure and virulence-associated traits of *P. ananatis* isolated from rice using a combination of comparative genomics and phenotypic assays. We show that rice-isolated strains segregate into two distinct genomic lineages that differ in host range and virulence factor composition. We further demonstrate that the HiVir operon contributes to necrotic symptom development in rice but is not required for bacterial replication within rice tissue. Together, these findings reveal that symptom development and bacterial proliferation can be uncoupled in this pathosystem and provide new insight into how lineage-specific genomic variation shapes host specialization in this emerging pathogen.

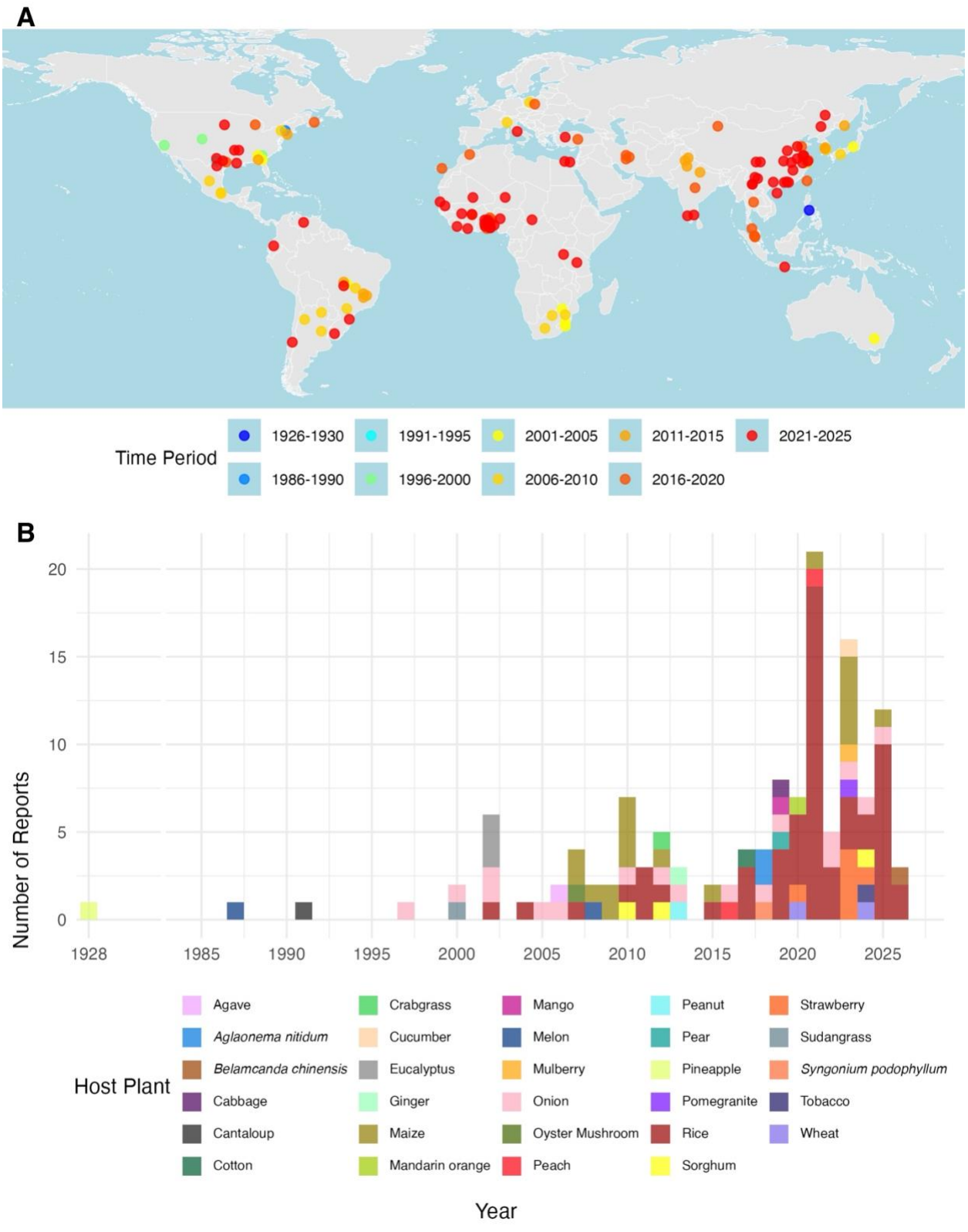
A
Time Period
1926-1930
1986-1990
1991-1995
1996-2000
2001-2005
2006-2010
2011-2015
2016-2020
2021-2025
B
Number of Reports
0
5
10
15
20
1928
1985
1990
1995
2000
2005
2010
2015
2020
2025
Year
Host Plant
Agave
Aglaonema nitidum
Belamcanda chinensis
Cabbage
Cantaloup
Cotton
Crabgrass
Cucumber
Eucalyptus
Ginger
Maize
Mandarin orange
Mango
Melon
Mulberry
Onion
Oyster Mushroom
Peach
Peanut
Pear
Pineapple
Pomegranite
Rice
Sorghum
Strawberry
Sudangrass
Syngonium podophyllum
Tobacco
Wheat

**Fig. 1. A,** World map illustrating the global distribution of reported plant diseases caused by *P. ananatis* across diverse plant hosts. Dot color represents peer-reviewed publication year. Geographic coordinates were extracted from the metadata of peer-reviewed publications (approximate coordinates were estimated when not provided). **B,** Temporal distribution of disease reports of *P. ananatis* by host species. Colors denote different agricultural crops from which the pathogen was isolated.

## Materials and Methods

### Mapping incidence and spread of *P. ananatis* as a pathogen

A comprehensive search of peer-reviewed literature on *P. ananatis* associated with plant disease was used to generate a map of the pathogen's geographic distribution (Fig. 1A, Table S1). The publication date was used to resolve temporal dynamics. For each report, the host species was identified (Fig. 1B, Table S1). We included reports of *Erwinia ananas, Erwinia uredevora,* and *Pantoea ananas,* as all are now classified as *P. ananatis* (Mergaert et al. 1993). We did not include reports of *Erwinia herbicola,* as it was reclassified to *P. agglomerans* (Gavini et al. 1989).

### Isolation of *P. ananatis* from symptomatic rice tissue

In 2021 and 2024, symptomatic rice leaf tissue was collected from rice grown in global germplasm research plots at the Dale Bumpers National Rice Research Center (DBNRRC) in Stuttgart, AR, as well as from infected seeds at the Rice Research and Extension Center (RREC) at the University of Arkansas. When grown in the greenhouse, rice variety JiBoYa showed the same characteristic symptoms of *Pantoea* leaf blight and *Pantoea* panicle blight that were present in the field (Fig. S1) Bacterial isolation of field samples was performed at Colorado State

University (CSU) and the DBNRRC. Soakate from symptomatic leaves was plated on nutrient agar (NA) as previously reported (Luna et al. 2023).

**Whole-genome sequencing of *P. ananatis* strains**

Bacterial strains were grown overnight in liquid Luria-Bertani (LB) medium at 30°C while shaking. Genomic DNA was extracted from each strain using the Zymo High Molecular Weight (HMW) DNA Extraction Kit (Zymo Reseach, USA) according to the manufacturer's protocol, with modifications to include both Lysozyme A and Proteinase K treatment during cell lysis to optimize DNA yield and integrity for long-read sequencing.

A total of 12 *P. ananatis* strains were sequenced (Table 1). Purified genomic DNA from each strain was sequenced using either hybrid sequencing with Illumina short-read and PacBio long-read technologies (three strains; AR358, JEL0889, JEL0890, sequenced in 2024 at North Carolina State University) or hybrid sequencing with Illumina short-read and Oxford Nanopore long-read technologies (nine remaining strains, Plasmidsaurus, USA, sequenced in 2025). Sequencing libraries were prepared by the service providers according to standard protocols. Genomes were deposited to NCBI under BioProject PRJNA1454052.

For PacBio and Illumina hybrid sequencing, DNA was quantified using a Qubit 4 Fluorometer (ThermoFisher Scientific, USA) and fragmented with Covaris g-TUBES according to PacBio specifications. Sequencing libraries were prepared using the PacBio SMRTbell prep kit 3.0 and SMRTbell barcoded adapter plate 3.0. The pooled libraries were bound using the Sequel II binding kit 3.2 and sequenced on an in-house PacBio Sequel IIe instrument configured to capture subreads and kinetics data. On-instrument demultiplexing, quality control, and adapter

trimming were performed using Lima (PacBio). HiFi sequencing output in BAM format was converted to FastQ format using SamTools Fastq (Danecek et al. 2021).

Illumina libraries were prepared using the Illumina DNA prep kit with Integrated DNA Technologies 10 bp unique dual indices, and sequencing was performed on an Illumina NovaSeq X Plus sequencer generating 2x151 bp paired-end reads (SeqCenter, USA). Demultiplexing, quality control, and adapter trimming were completed using bcl-convert v4.2.4 (Illumina).

Genomes sequenced using PacBio and Illumina were assembled, rotated and trimmed with the Trycycler v0.5.4 long-read consensus assembler (Wick et al. 2021) using default parameters. Briefly, long reads were assembled with Flye v2.9.5-b1801 (Kolmogorov et al. 2019), miniasm 0.3-r179 and minipolish v0.1.2 (Li 2016), and Raven v1.8.3 (Vaser and Šikić 2021). The resulting assembly was polished with Illumina reads using polypolish v0.6.0 (Wick and Holt 2022). Genome completeness and contamination were assessed using CheckM v1.2.3 (Parks et al. 2015) and all genomes were > 99.5% complete with < 0.3% contamination.

For ONT and Illumina hybrid sequencing through Plasmidsaurus, long-read libraries were constructed using an amplification-free protocol with v14 library preparation chemistry with minimal DNA fragmentation in a sequence-independent manner via tagmentation and sequenced on R10.4.1 flow cells using a primer-free protocol. Short-read sequencing consisted of paired-end 2x150 bp Illumina reads.

Raw ONT reads were basecalled using Dorado v4.3 (Oxford Nanopore Technologies) with default Q10 quality filtering. Reads shorter than 300 bp were removed and the 95% highest quality remaining reads were retained using Filtlong v0.2.1 (github.com/rrwick/Filtlong). Genome size was estimated with Lrge v0.2.1 (Hall et al. 2025). Downsampling generated

subsampled read sets at optimal coverage using Autocycler (Wick et al. 2025). Assemblies were produced using three assemblers: Flye v2.9.6 (Kolmogorov et al. 2019) with parameters optimized for high-accuracy ONT reads, Hifiasm (Cheng et al. 2021), and Plassembler v1.8.0 (Bouras et al. 2023) for plasmid detection and assembly. Autocycler was used to compress, cluster, trim, resolve, and generate a consensus assembly across all assemblers, and assemblies were rotated to an optimal start position using dnaapler (Bouras et al. 2024).

For hybrid polishing, Illumina short reads were quality-filtered using fastp (Phred ≥ 15, length ≥ 50 bp, with adapter and poly-G trimming) (Chen et al. 2018) and aligned to the long-read assembly using bwa-mem2 (Vasimuddin et al. 2019). The assembly was then polished with Polypolish v0.6.0 (Wick and Holt 2022). Genome completeness and contamination were assessed with CheckM v1.2.2 (Parks et al. 2015), and all genomes were > 99.5% complete with < 0.8% contamination, with the exceptions of JEL0891 (3.23% contamination) and PP094-PanT1S3 (11.66% contamination). Assemblies were annotated using Bakta v1.11 (Schwengers et al. 2021). Sequencing statistics can be found in table S2.

**Mapping genome relatedness**

To investigate genomic relatedness among *P. ananatis* strains, an Average Nucleotide Identity (ANI) analysis was conducted using both publicly available genomes downloaded from NCBI on January 19, 2026, and the genomes sequenced in this study.

ANI calculations were performed using pyani v0.2.12 (Pritchard et al. 2016). Genome assemblies were formatted as FASTA files and analyzed using the ANIm method with default parameters. Pairwise ANI values were computed for all genome combinations to generate a similarity matrix representing genomic relatedness across the dataset. Additionally, pairwise ANI

values were computed for genomes of rice-isolated strains to better visualize relationships within the rice pathosystem. The resulting ANI matrices (Tables S3, S4) were imported into R (v4.5.2) for visualization. Heatmaps and hierarchical clustering dendrograms were constructed using the pheatmap package (v1.0.13). For all *P. ananatis* strains analyzed with pyani, NCBI GCF accession, strain name, host, and ANI-derived lineage were identified (Table S5).

**Comparative pangenome analysis using Roary**

To characterize genetic differences between the rice-associated and generalist lineages of *P. ananatis*, a comparative pangenome analysis was performed using Roary, Galaxy version 3.13.0 (Galaxy 2024; Page et al. 2015). All publicly available genomes from rice-isolated strains were downloaded as FASTA sequences and were re-annotated using Bakta, Galaxy version 1.9.4 (Galaxy 2024; Schwengers et al. 2021) alongside the genomes assembled in this study for consistency in genomic comparisons. Gene presence/absence heatmaps were generated using Python v3.14.3.

To identify genes associated with each *P. ananatis* lineage, a pan-genome-wide association study (pan-GWAS) was conducted using Scoary, Galaxy version 1.6.16 (Brynildsrud et al. 2016; Galaxy 2024). The pan-genome presence/absence matrix generated by Roary was used as input, with lineage membership (generalist or rice-associated) annotated in a trait file. Genes that showed complete disparity between lineages (present in all genomes of one lineage, completely absent from the other) were functionally annotated using eggNOG-Mapper, Galaxy version 5.0.2 (Cantalapiedra et al. 2021; Galaxy 2024). Here, representative nucleotide sequences for each lineage-associated gene were extracted from the Roary pan-genome reference file, translated to amino acid sequences, and submitted for annotation, with seed orthologues

computed with DIAMOND (Buchfink et al. 2015; Galaxy 2024), Galaxy version 2.1.25, in sensitive mode and only experimentally (non-computational) curated terms.

**Characterizing HiVir and *alt* presence in rice-isolated *P. ananatis***

A library of 79 isolates collected from symptomatic tissue in Arkansas in 2021 and 2024 was first screened to confirm *P. ananatis* identity using the PANA1080 primer set (Asselin et al. 2016; Shin et al. 2022). Among confirmed *P. ananatis* isolates, HiVir operon presence was assessed using the HiVir2p primer set, which amplifies functional genes within the operon. This primer set targets the junction between *hvrA* and *hvrB,* where common SNPs leading to nonfunctional operons occur (Stice et al. 2021) (Fig. S2).

To determine HiVir presence across all publicly available *P. ananatis* rice-isolates, as well as the genomes generated in this study, HiVir protein sequences from strain PNA_97-1R (Stice et al. 2018) were used as queries in a local protein cluster BLAST search with cblaster v1.4.0 (Gilchrist et al. 2021). These sequences were searched against annotated sequences from the genomes of 57 rice-isolated strains to identify homologous genes and assess HiVir operon completeness (Table S6).

To assess the conservation of the *alt* gene cluster among *P. ananatis* rice isolates, the *alt* gene cluster sequence was downloaded from NCBI using locus tags for each gene in the pOVR plasmid in strain PNA97-1R (Stice et al. 2020). Each gene (*altA-altE, altG-altJ, altR,* and *gorB*) was used as a query to search all genomes of rice-isolated strains (publicly available and newly sequenced) using cblaster v1.4.0 (Gilchrist et al. 2021). Two control genomes from strains isolated from onion containing the *alt* cluster, PNA 15-1 (NCBI accession GCF_002959585.1), and PNA 200-3 (NCBI accession GCF_002959565.1) were used as controls (Table S7).

**Construction of HiVir mutants in *P. ananatis***

Deletion mutants of *hvrB* and *hvrF* were generated in *P. ananatis* strain PP105 using biparental conjugation followed by allelic exchange. Allelic exchange plasmids pR6KT2G::Δ*hvrB* and pR6KT2G::Δ*hvrF* (Shin et al. 2023), each conferring gentamicin resistance ($Gm^R$) and carrying the counter-selection markers *sacB* and *lacZ*, were maintained in *Escherichia coli* strain Rho5 (DAP auxotrophic). Complementation plasmids pBS46::nComp*hvrB* and pBS46::nComp*hvrF* (Shin et al. 2023), conferring resistance to kanamycin ($Km^R$), were maintained in *E. coli* strain MaHI (Table S8).

For allelic exchange, donor *E. coli* Rho5 strains carrying the appropriate plasmid and recipient *P. ananatis* PP105 were grown in LB overnight at 30 °C with shaking. Cultures were pelleted, washed with 1X PBS to remove antibiotics, and mixed at a 1:1 ratio. Cell mixtures were spotted onto LB agar plates supplemented with 400 μg/ml diaminopimelic acid (DAP) and incubated at 30°C overnight.

Following mating, cells were scraped from the LB+DAP plates, resuspended in sterile 1X PBS and plated onto LB agar containing 15 μg/ml gentamicin to select for *P. ananatis* transconjugants and counter select against the *E. coli* donor. Gentamicin-resistant colonies were isolated and cultured in LB broth supplemented with sucrose overnight to induce *sacB*-mediated counterselection and promote resolution of the allelic exchange.

Sucrose-treated cultures were serially diluted and plated onto LB agar containing X-gal to screen for loss of the plasmid backbone via *lacZ* counterselection. White colonies were screened by PCR with *hvrB* and *hvrF*-specific primer sets followed by Sanger sequencing (Azenta Life

Sciences, USA) to confirm successful allelic exchange (Fig. S3), yielding unmarked Δ*hvrB* and Δ*hvrF* deletion mutants.

Complementation strains were generated by the introduction of the corresponding *hvrB* and *hvrF* complementation plasmids into confirmed deletion mutants. Plasmids pBS46::nComp*hvrB* and pBS46::Comp*hvrF* were first isolated from *E. coli* strain MaHI using the ThermoFisher GeneJet Plasmid MiniPrep kit (ThermoFisher Scientific, USA). Electrocompetent cells of the Δ*hvrB* and Δ*hvrF* mutant strains were transformed by electroporation using a Bio-Rad Micropulser (Bio-Rad Laboratories, USA) at 1.8 kV for 5 ms with 200 ng of the purified plasmids in a 0.1 cm cuvette (Alkali Scientific, USA). Transformants were recovered in non-selective LB broth and plated on LB agar containing 50 µg/ml kanamycin to select for complemented strains. Successful plasmid introduction was confirmed by PCR and antibiotic resistance screening.

*In vitro* growth curves were performed for each mutant/complement pair (PP105Δ*hvrB* and PP105Δ*hvrF*, with their corresponding complemented strains) alongside the wild-type control. Experiments were conducted in LB broth to assess whether the mutations affected bacterial growth compared to the wild type. For complemented strains, growth curves were performed both in the presence of 25 µg/ml kanamycin to assess potential effects of plasmid maintenance on bacterial growth.

Overnight cultures were inoculated into fresh medium and diluted to a starting optical density of approximately 0.05 at 600 nm ($OD_{600}$). Diluted cultures were pipetted into Costar flat-bottom, transparent 96-well microplates and placed into a Tecan Infinite M Nano Plus microplate reader (Tecan Life Sciences, Switzerland) at 30°C with continuous orbital shaking at 213 rpm. Cell density ($OD_{600}$) was recorded at regular intervals throughout the experiment. Each strain was

represented by five technical replicates per plate, including five reps for a blank, containing just LB (Fig. S4).

**Plant inoculations**

*In planta* growth assays were performed using rice (*Oryza sativa*) variety Azucena to evaluate the virulence and colonization of *P. ananatis* strains. To promote expression of virulence-associated factors prior to inoculation, bacterial cultures were grown overnight in mCLM medium (Asselin et al. 2018) at 30°C with shaking. Cells were harvested by centrifugation, washed three times with 1mM $MgCl_2$, and the final pellets were resuspended in sterile distilled water and adjusted to an $OD_{600}$ of 0.2. The starting inoculum was serially diluted and plated on NA to determine bacterial numbers ($log_{10}$CFU).

The second and third fully expanded rice leaves were infiltrated using a needleless syringe as previously described (Reimers and Leach 1991). At 6, 12, 24, and 48 hours post-inoculation (hpi), and after symptom development (10 days post-inoculation, dpi), leaf tissue was harvested for bacterial enumeration.

To assess bacterial numbers, a 6 cm section of leaf tissue surrounding the infiltration site was excised and placed into 2 ml Safe-Lock tubes containing 500 µl sterile distilled water and two stainless-steel beads. Samples were disrupted using a Qiagen TissueLyser II (Qiagen, Germany). Plant debris was pelleted by centrifugation at 400 xg for 1 min, and the resulting supernatant was serially diluted and plated onto NA. After incubation at 30 °C for 24 h, colonies were counted to determine bacterial numbers.

Inoculua for infiltration of *Nicotiana benthamiana* and onion was prepared as described above. Bacterial suspensions were infiltrated into the abaxial side of *N. benthamiana* leaves and the infiltration spread was marked with a Sharpie. Symptom development was assessed at 7 dpi.

Onion inoculations were performed by purchasing red onions from a local supermarket, and using methods previously described (Stice et al. 2018). Inoculations occurred by pipetting 10 µl of inoculum ($OD_{600}$ of 0.1) onto wounds created with pipette tips on the inner surface of onion scales after surface sterilization (3% bleach solution, two washes in sterile, distilled water).

To quantify bacterial replication over time, a 1 cm diameter cork borer was used to punch tissue from the scale surrounding the inoculation site. For each sampling time, tissue was crushed in 2 mL Eppendorf Safe-Lock tubes with two stainless steel beads and 500 µl of sterile water by shaking in a Qiagen TissueLyser II at 30 rps for 1 min. Plant debris was pelleted by centrifugation at 400 xg for 1 min and the supernatant was serially diluted and plated onto NA. Bacterial numbers were determined after incubation at 30°C for 24 h.

*In planta* growth curves of *P. ananatis* in rice were fit to a linear mixed-effects model with the lme4 package in R, with bacterial numbers as the response variable. Fixed effects included inoculum strain (WT PP105 or JEL0890 for lineage comparison; WT PP105, PP105Δ*hvrB* or PP105Δ*hvrF*, PP105Comp*hvrB* or PP105Comp*hvrF* for HiVir mutant comparisons), time post inoculation (hpi), and leaf position, while plant was included as a random effect to account for non-independence among leaves from the same plant.

The *in planta* growth curves of *P. ananatis* in onion were fit to a linear regression model with bacterial counts as the response variable, inoculum strain (PP105, PP105Δ*hvrB*, PP105Comp*hvrB*, and JEL0890 for mutant analysis; JEL0890, PP088, AR358, PP0893,

JEL0891, and PP105 for comparison of lineages), and time post-inoculation as fixed effects. All samples were independent, eliminating the need for random effects.

## Results

### A distinct lineage of *P. ananatis* is specific to rice

Relationships among publicly available and newly sequenced *P. ananatis* genomes (n = 326) were assessed using ANI which resolved two distinct clusters (274 and 52 genomes, respectively) at a 98.5% ANI threshold. The smaller cluster was composed largely of strains recovered exclusively from rice (rice-associated lineage) and had an average within-group pairwise ANI of 99.26% (standard deviation (SD) = 0.16%) with an average coverage of 91.1% (SD = 3.0%). The second, larger cluster included strains from multiple plant hosts, including a subset from rice (generalist lineage), and had an average within-group pairwise ANI of 99.21% (SD = 0.14%) with an average coverage of 90.7% (SD = 3.3%). Between group average ANI was 96.63% (SD = 0.06%) with an average coverage of 85.6% (SD = 2.5%) (Fig. 2A). When the analysis was restricted to genomes of *P. ananatis* isolated only from rice (n = 57), the same clustering pattern was observed. All genomes within the rice-associated lineage (n = 40) grouped together (average ANI 99.28%, SD = 0.18%; average coverage 91.2%, SD = 3.5%), while the remaining rice-derived genomes (n = 17) clustered with the broader generalist lineage (average ANI 99.19%, SD = 0.06%; average coverage 89.4%, SD = 3.3%) with between group average ANI of 96.62% (SD = 0.05%) and average coverage of 87.7% (SD = 3.0%) (Fig. 2B). All pairwise comparisons from both analyses exceeded the 96% ANI species threshold. Notably, rice-derived strains of *P. ananatis* were distributed across both lineages, indicating that strains

recovered from rice can differ substantially in their genomic background and associated gene content. These results raise the question of whether these lineages differ not only in genomic composition, but in strategies employed for successful infection of rice.

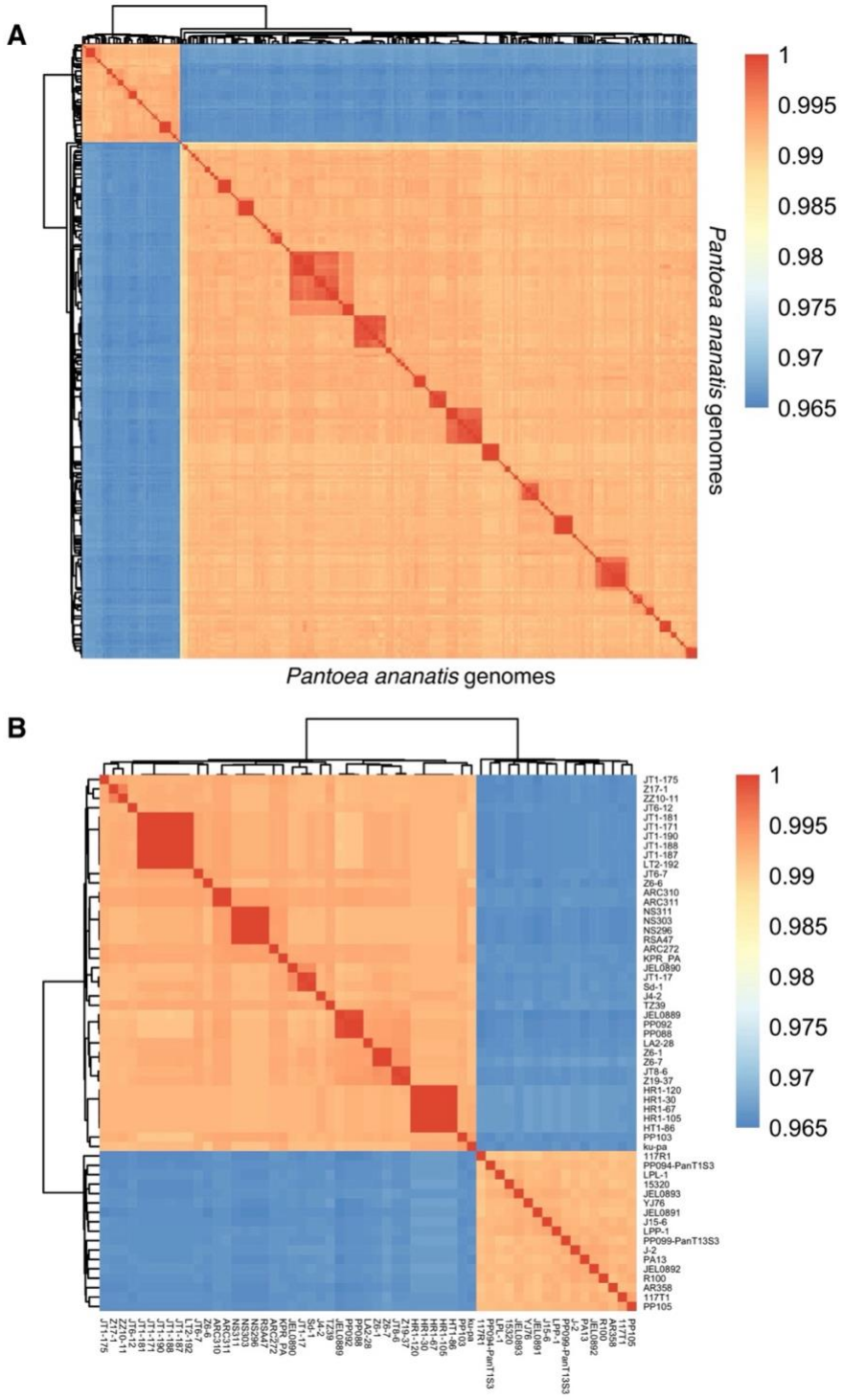

**Fig. 2.** Genomic similarity of *P. ananatis* conducted using pyani. **A,** Average Nucleotide Identity (ANI) of publicly available *P. ananatis* genomes, including those downloaded as FASTA files from NCBI, and the 12 genomes sequenced in this study (total n=326). Expansion of Fig. 2A for enhanced resolution in shown in Fig. S2. **B,** ANI of publicly available and newly sequenced *P. ananatis* genomes of strains isolated from rice only (n=57).

**Comparative genomics reveals lineage-specific gene content**

To further characterize genomic features distinguishing the two lineages, a pangenome analysis was conducted using Roary on genomes of 57 total rice-isolated *P. ananatis* strains, including the newly sequenced strains and publicly available datasets. Gene presence-absence patterns were examined in the context of ANI-defined clusters to identify genes conserved within the rice-associated group but absent or rare in generalist strains, and vice versa. A total of 16,533 genes were identified across the pangenome. Of these, 587 genes were differentially present between the two lineages, defined as present in at least 80% of genomes in one lineage and less than 20% in the other (Fig. 3A). The Scoary pan-GWAS identified 178 genes present in 100% of generalist genomes and absent from all rice-associated genomes, while 114 genes were present in 100% of the rice-associated genomes and absent from all generalist genomes (Tables S9, S10). These lineage-specific differences in gene content provide insights into mechanisms of host specialization and can be used for future development of molecular tools for lineage discrimination.

To gain insight into the putative functional roles of lineage-specific genes, we performed functional annotation using eggNOG-Mapper. This method successfully annotated 160 of the 178 generalist genes and 106 of the 117 rice-associated genes. Despite the identification of hundreds of lineage-specific genes, significant overlap of clusters of orthologous genes (COG) categories was observed. However, two unique COG groups were identified among the

generalist lineage genes (defense mechanisms and cell cycle control, cell division, chromosome partitioning) (Fig. 3B, Table S11).

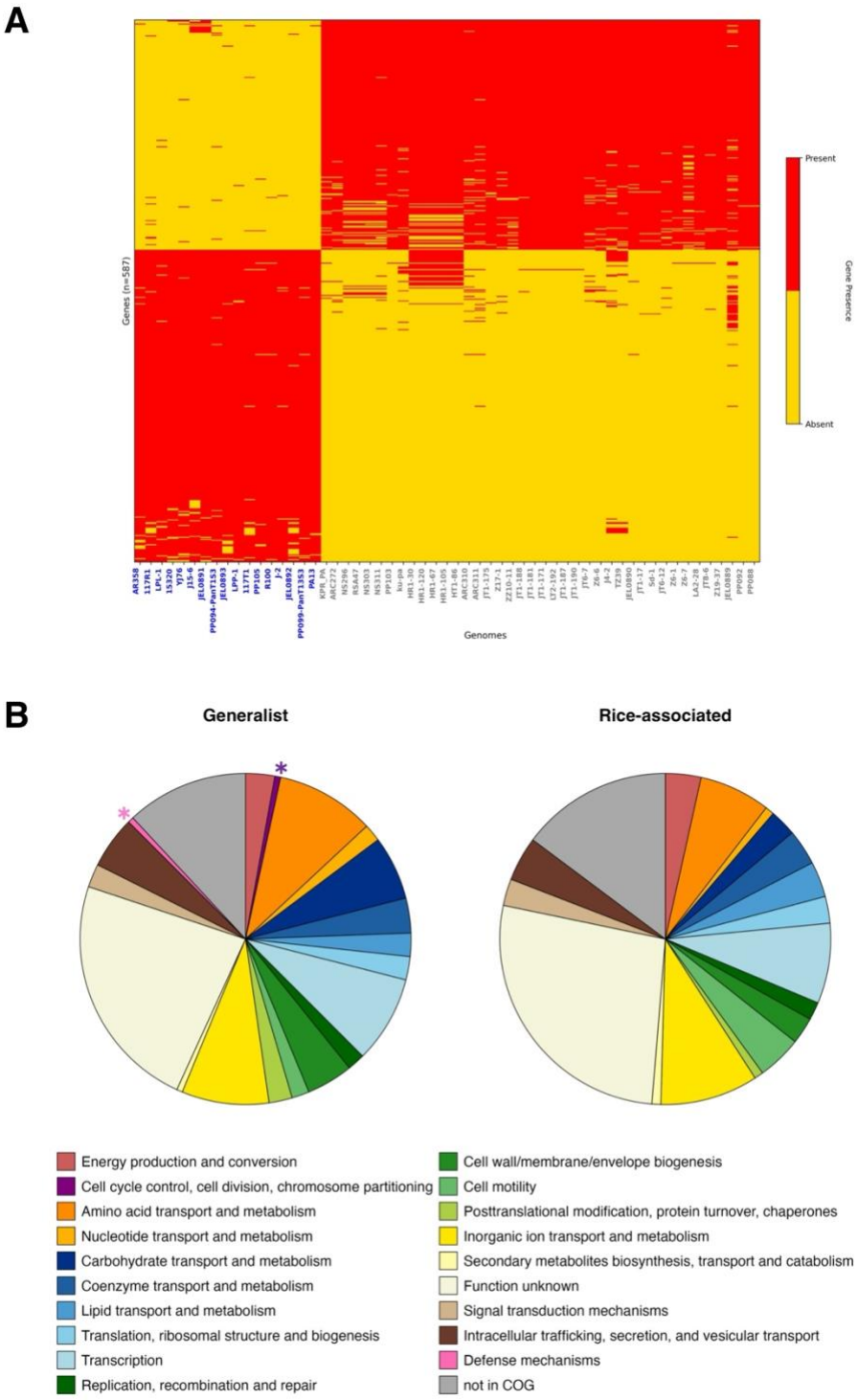

**Fig. 3.** A pangenome analysis on rice-isolated *P. ananatis* strains (n=57) using Roary. Scoary pan-GWAS identified genes unique to each lineage and COG categories of unique genes was assigned with eggNOG Mapper. **A,** Heatmap of genes enriched in each lineage (appear in >80% of genomes in one lineage, <20% in the other). **B,** Functional annotation of genes unique to each lineage using eggNOG Mapper.

**Pathogenicity and growth of *P. ananatis* lineages in rice**

When strains from the distinct lineages (PP105, generalist; JEL0890, rice-associated) were inoculated into the 2$^{nd}$ and 3$^{rd}$ fully expanded leaves of 4-week-old rice plants, clear differences in symptom development emerged. Inoculation with PP105 resulted in spreading necrotic lesions, whereas JEL0890 did not cause visible necrosis (Fig. 4B).

Despite these contrasting symptom phenotypes, both strains exhibited comparable *in planta* growth dynamics. Type II Wald chi-square tests revealed a strong effect of time post-inoculation ($\chi^2 = 105.39$, df = 3, $p < 0.001$), consistent with active bacterial multiplication within leaf tissue (Fig. 4A). However, neither strain genotype ($\chi^2 = 0.92$, df = 1, $p = 0.337$) nor leaf position ($\chi^2 = 1.30$, df = 1, $p = 0.254$) significantly influenced bacterial population sizes. Likewise, no significant interactions were detected among strain, time, and leaf position (strain x time: $\chi^2 = 2.72$, df = 3, $p = 0.605$; time x leaf: $\chi^2 = 2.68$, df = 4, $p = 0.613$; three-way interaction: $\chi^2 = 0.93$, df = 4, $p = 0.921$). A modest within-strain difference was observed in leaf position for PP105, with bacterial numbers higher in the second leaf relative to the third ($\chi^2 = 4.36$, df = 1, $p = 0.037$).

Taken together, these results indicate that PP105 and JEL0890 achieve similar population sizes and replication kinetics within rice tissue despite marked differences in symptom development. This demonstrates that the lineage-specific differences are reflected in symptom

expression, but not in bacterial proliferation (Fig. 4A), indicating that these traits can be uncoupled during infection of rice.

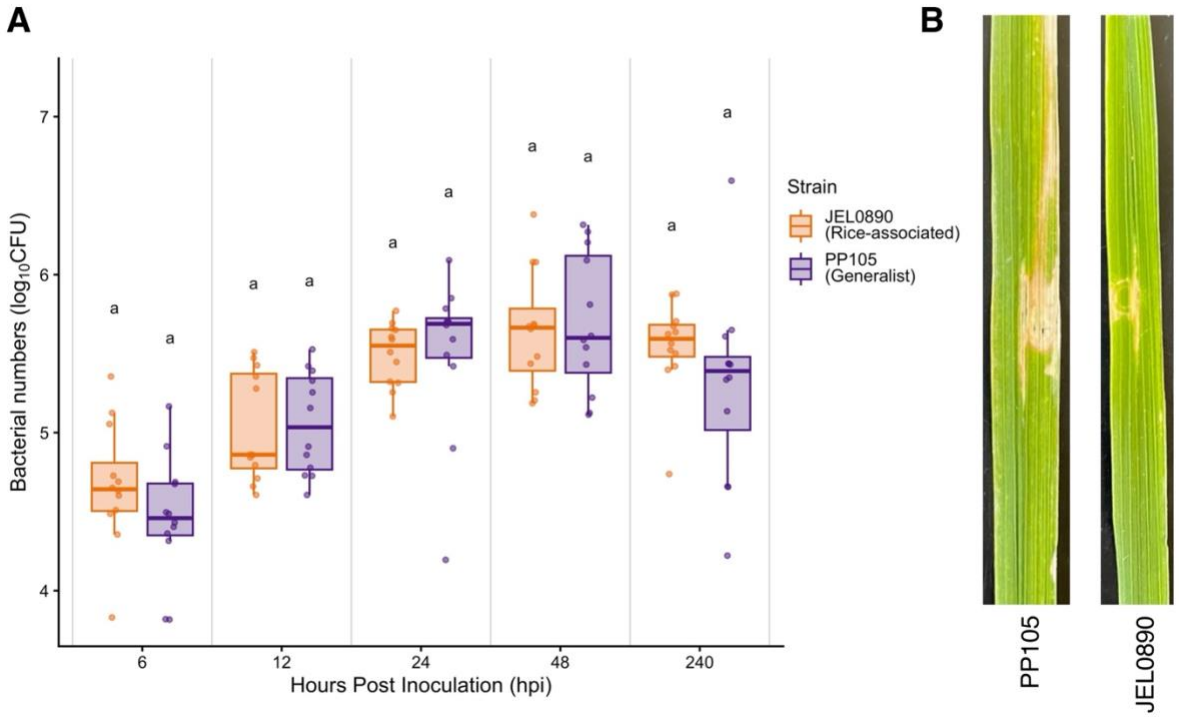


**Fig. 4.** *P. ananatis* generalist strain PP105 and rice-associated strain JEL0890 inoculated into leaves of 4-week-old rice (variety Azucena). **A,** Growth curve of PP105 and JEL0890 strains extracted from 6 cm rice leaf sections including the infiltration site at 6, 12, 24, 48, and 240 hpi. Starting inoculum densities were 8.40 and 8.36 log10CFU/ml, respectively. Letters indicate significant differences measured at $p < 0.05$. **B,** Symptom development of rice leaves inoculated with PP105 and JEL0890. Images taken 240 hpi.

**HiVir operon is unequally distributed across *P. ananatis* lineages**

Given the observed differences in symptom development between lineages despite similar bacterial population sizes, we next examined whether known virulence-associated genes differed in their distribution across these groups.

Pantaphos, a phosphonate-type toxin produced by some pathogenic *P. ananatis* strains, was first described as important for necrotic lesion development in onion (Asselin et al. 2018). Toxin production depends on the presence of the HiVir operon, an 11-gene cluster (*hvrA-hvrK),* including six genes (*hvrA-hvrF*) required for biosynthesis and a transporter gene (*hvrI)* (Polidore et al. 2024). Mutations in nearly any gene within the operon was shown to impair lesion development (Shin et al. 2023).

To determine the distribution of the HiVir operon in rice-associated *P. ananatis*, we screened both sequenced genomes and field isolates. None of the genomes from rice-isolated strains within the rice-associated lineage contained the operon (0/40), while it was present in 11 of 17 genomes from rice-isolated generalist strains (Table S6). We further screened isolates collected from symptomatic rice tissue in Stuttgart, Arkansas. The HiVir operon was detected in 5 of 37 isolates collected in 2021 and 9 of 26 isolates collected in 2024 using PCR-based diagnostics (Fig. S2). Although most isolates were not assigned to lineages via whole-genome sequencing, both HiVir-positive and HiVir-negative isolates were identified in field samples, including isolates from both lineages within the same symptomatic leaf tissue.

**Effect of HiVir on symptom development in *Nicotiana benthamiana***

To assess the contribution of the HiVir operon to symptom development, deletion mutants were generated in two genes required for pantaphos biosynthesis, *hvrB* and *hvrF*. The *hvrB* gene encodes a flavin-dependent mono-oxogenase that catalyzes the hydroxylation of Methyl-PMME with the aid of HvrK, and *hvrF* encodes an O-methyltransferase responsible for SAM-dependent methylation of pantaphos (Fig. 5A) (Polidore et al. 2024). Complemented strains were generated by introducing functional copies of each gene into the respective mutants.

Wild-type (WT) PP105 induced a necrotic response in *N. benthamiana* leaves by 7 dpi. In contrast, necrosis was not observed in leaves inoculated with PP105Δ*hvrB* or PP105Δ*hvrF* mutants. Complemented strains restored the ability to induce necrosis, although the response was reduced relative to WT (Fig. 5B). All sequenced strains were also tested for their ability to induce necrosis in *N. benthamiana.* Necrotic symptoms were observed only in response to strains that tested positive for the HiVir operon (Fig. 5C).

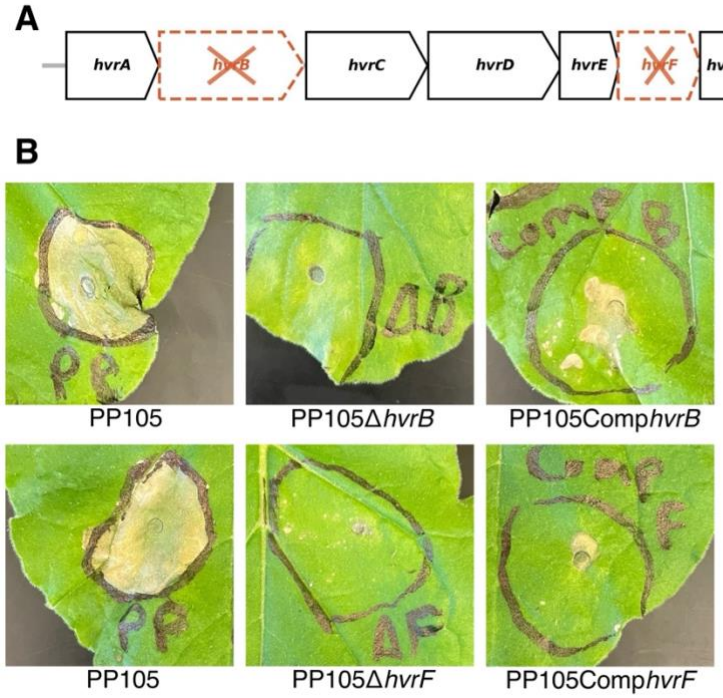


C

1 kb

| Strain | Necrosis | HiVir |
|---|---|---|
| AR358 | - | - |
| JEL0889 | - | - |
| JEL0890 | - | - |
| JEL0891 | + | + |
| JEL0892 | + | + |
| JEL0893 | - | - |
| PP088 | - | - |
| PP092 | - | - |
| PP094-PanT1S3 | + | + |
| PP099-PanT13S3 | + | + |
| PP103 | - | - |
| PP105 | + | + |

**Fig. 5. A,** Targets for mutagenesis via allelic exchange within the HiVir operon. **B,** *N. benthamiana* showing necrosis phenotype for WT PP105, deletion mutants (PP105Δ*hvrB*; PP105Δ*hvrF*), and complemented strains at seven dpi. C, *N. benthamiana* phenotype for WT strains sequenced for this study, HiVir presence determined via PCR with HiVir2p primer set (Stice et al. 2021).

**Table 1**. *P. ananatis* strains used and sequenced in this study.

| Strain | Isolation year | Host variety | Plant tissue | Sequencing technology | NCBI BioSample ID | Reference |
|---|---|---|---|---|---|---|
| AR358 | 2021 | JiBoYa | Leaf | PacBio | SAMN57290340 | Luna et. al. 2023. |
| JEL0889 | 2021 | JiBoYa | Leaf | PacBio | SAMN57290335 | This study |
| JEL0890 | 2021 | Desconhecido Come Cru | Leaf | PacBio | SAMN57290336 | This study |
| JEL0891 | 2021 | Desconhecido Come Cru | Leaf | Hybrid | SAMN57290337 | This study |
| JEL0892 | 2021 | JiBoYa | Leaf | Hybrid | SAMN57290338 | This study |
| JEL0893 | 2021 | JiBoYa | Leaf | Hybrid | SAMN57290339 | This study |
| PP088 | 2024 | JiBoYa | Leaf | Hybrid | SAMN57290341 | This study |
| PP092 | 2024 | JiBoYa | Leaf | Hybrid | SAMN57290342 | This study |
| PP094-PanT1S3 | 2024 | JiBoYa | Seed | Hybrid | SAMN57290343 | Pedrozo et. al. *Unpub.* |
| PP099-PanT13S3 | 2024 | RUI201145 | Seed | Hybrid | SAMN57290344 | Pedrozo et. al. *Unpub.* |
| PP103 | 2024 | RUI201145 | Seed | Hybrid | SAMN57290345 | Pedrozo et. al. *Unpub.* |
| PP105 | 2024 | RUI201145 | Seed | Hybrid | SAMN57290334 | de Paula et. al. 2026. |

**HiVir presence determines necrotic symptom development in rice**

To examine the role of the HiVir operon in rice, WT PP105, PP105Δ*hvrB* and PP105Δ*hvrF* mutants, and their complemented strains were infiltrated into the 2nd and 3rd fully expanded leaves of 4-week-old rice leaves. At 10 dpi, WT and complemented strains produced localized necrosis at the site of infiltration. In contrast, leaves inoculated with PP105Δ*hvrB* and PP105Δ*hvrF* mutants exhibited substantially reduced necrosis (Fig. 6B, 6D).

**Pantaphos is dispensable for bacterial replication in rice tissue**

Despite differences in symptom development, bacterial growth *in planta* was similar among strains (Fig. 6A, 6C). However, at standardized optical density, complemented strain inocula yielded lower bacterial counts, likely reflecting antibiotic selection during culture.

Results from Type II Wald chi-square tests on data recovered from the PP105Δ*hvrB* experiment showed that inoculum strain had a significant main effect ($\chi^2 = 120.91$, df = 2, $p < 0.001$), as did time point ($\chi^2 = 423.85$, df = 4, $p < 0.001$) and leaf position ($\chi^2 = 10.94$, df = 1, $p < 0.001$). A significant strain by time interaction ($\chi^2 = 69.14$, df = 8, $p < 0.001$) was indicative of difference in growth dynamics across the time course of the experiment, however no significant

differences in bacterial population size were detected between WT and PP105Δ*hvrB* across the entire time course ($p = 0.956$). The complemented strain (PP105Comp*hvrB*) exhibited lower bacterial populations at early time points (6 and 12 hpi; $p < 0.001$), but populations converged by 48 hpi, with no differences among strains (all $p > 0.262$). All strains reached similar maximum population sizes (Fig. 5A).

Results from the PP105Δ*hvrF* experiment revealed significant main effects of inoculum strain ($\chi^2 = 136.55$, $df = 2$, $p < 0.001$) and time point ($\chi^2 = 887.44$, $df = 4$, $p < 0.001$), whereas leaf position was not significant ($\chi^2 = 0.75$, $df = 1$, $p = 0.386$). A significant strain by time interaction ($\chi^2 = 118.62$, $df = 8$, $p < 0.001$) and a three-way interaction (strain x time x leaf position; $\chi^2 = 24.82$, $df = 8$, $p = 0.002$) were detected. As with PP105Δ*hvrB*, no differences in bacterial population size were observed between WT and PP105Δ*hvrF* across the time course ($p = 0.808$). The complemented strain (PP105Comp*hvrF*) showed reduced bacterial populations at early and mid-time points (6 - 24 hpi; $p < 0.001$), but populations converged by 48 hpi and remained similar at later time points (all $p > 0.587$). All strains reached peak bacterial population sizes at 48 hpi and declined by 240 hpi, with no differences in final population levels (Fig. 6C).

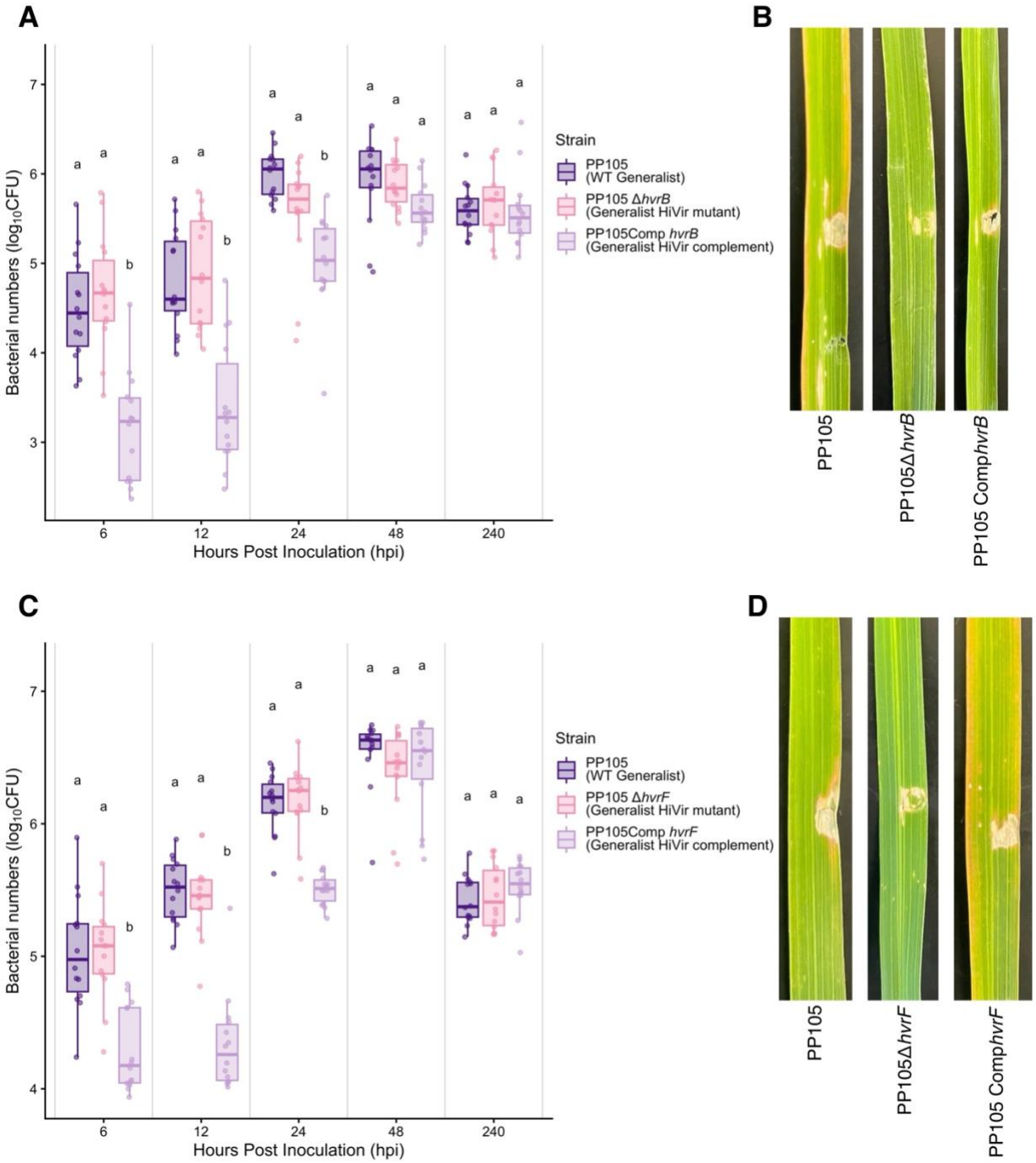


**Fig. 6.** *P. ananatis* generalist strain PP105, alongside HiVir deletion mutants (PP105Δ*hvrB*, PP105Δ*hvrF*) and complemented strains, inoculated into leaves of 4-week-old rice (variety Azucena). **A,** Multiplication of PP105, PP105Δ*hvrB*, and PP105Comp*hvrB* strains in rice leaves over time. Starting inoculum densities were 8.56, 8.46, and 7.18 log10CFU/ml, respectively. Bacteria were isolated from 6 cm rice leaf sections including the infiltration site at 6, 12, 24, 48,

and 240 hpi. Letters indicate differences measured at $p < 0.05$. **B,** Symptom development of rice leaves inoculated with PP105, PP105Δ*hvrB*, and PP105Comp*hvrB*. Images taken 240 hpi. **C,** Multiplication of PP105, PP105Δ*hvrF*, and PP105Comp*hvrF* strains in rice leaves over time. Starting inoculum densities were 7.93, 7.81, and 7.11 log10CFU/ml, respectively. Letters indicate differences measured at $p < 0.05$. **D,** Symptom development of rice leaves inoculated with PP105, PP105Δ*hvrF*, and PP105Comp*hvrF*. Images taken 240 hpi.

**In an alternate host, rice-associated *P. ananatis* exhibits reduced colonization relative to generalist strains**

To evaluate colonization in a non-rice host, strains from both lineages (PP105, generalist; JEL0890 rice-associated), along with PP105Δ*hvrB* and its complement, were inoculated into red onion scales (Fig. 7B). Type II F-tests revealed significant main effects of inoculum strain ($F = 63.80$, $df = 3$, $p < 0.001$) and time point ($F = 149.78$, $df = 4$, $p < 0.001$). A significant strain by time interaction ($F = 3.28$, $df = 12$, $p < 0.001$) indicated differences in growth dynamics among strains over the course of infection.

Within the HiVir-containing generalist strain iterations (PP105, PP105Δ*hvrB*, PP105Comp*hvrB*), bacterial loads were similar across most timepoints ($p > 0.05$), with modest differences observed at 48 hpi, where PP105 exhibited higher populations than PP105Comp*hvrB* and PP105Δ*hvrB* ($p = 0.003$, 0.020, respectively). By 72 hpi, no significant differences were detected among these strains (all $p > 0.05$). At early time points (6-24 hpi) PP105Comp*hvrB* exhibited bacterial populations comparable to both PP105Δ*hvrB* and WT PP105 (all $p > 0.05$).

In contrast, the HiVir-lacking strain JEL0890 from the rice-associated lineage consistently exhibited lower bacterial populations than all generalist strains across the entire time course (all $p < 0.05$). These differences were several orders of magnitude lower than those of all generalist strains, and these differences persisted through later time points (48-72 hpi) (Fig. 7A).

To determine if the difference in bacterial numbers between the generalist and rice-associated lineages is consistent when using additional strains, a panel of six wild-type strains were inoculated in onion scales and their growth was monitored over time. In this experiment, rice-associated strains JEL0890 and PP088, generalist strains containing HiVir, JEL0891 and PP105, and generalist strains lacking HiVir, AR358 and JEL0893 were used. Again, Type II F-tests revealed significant main effects of inoculum strain ($F = 36.31$, $df = 5$, $p < 0.001$), time point ($F = 156.74$, $df = 4$, $p < 0.001$), and strain by time interaction ($F = 2.11$, $df = 20$, $p = 0.007$). Overall, a reduction of bacterial numbers for rice-associated strains was observed compared to generalist strains. Specifically, JEL0890 had fewer bacterial numbers than all generalist strains at 24, 48, and 72 hpi (all $p < 0.05$), and was also significantly lower than AR358 and JEL0893 at 12 hpi ($p = 0.026$ and $p < 0.001$, respectively). PP088 showed a more variable pattern, differing significantly from JEL0893 at 12 hpi ($p = 0.007$), JEL0893, JEL0891, and PP105 at 48 hpi ($p < 0.001$, $p = 0.031$, and $p = 0.002$, respectively), and AR358, JEL0893, and PP105 at 72 hpi ($p = 0.004$, $p = 0.005$, and $p = 0.010$, respectively) (Fig. 7C). Additionally, in this experiment, we did not observe any differences in bacterial numbers among generalists that could be attributed to HiVir status, as pairwise contrasts between HiVir-containing generalists (JEL0891, PP105) and generalists lacking HiVir (AR358, JEL0893) were non-significant across all timepoints (all $p > 0.05$).

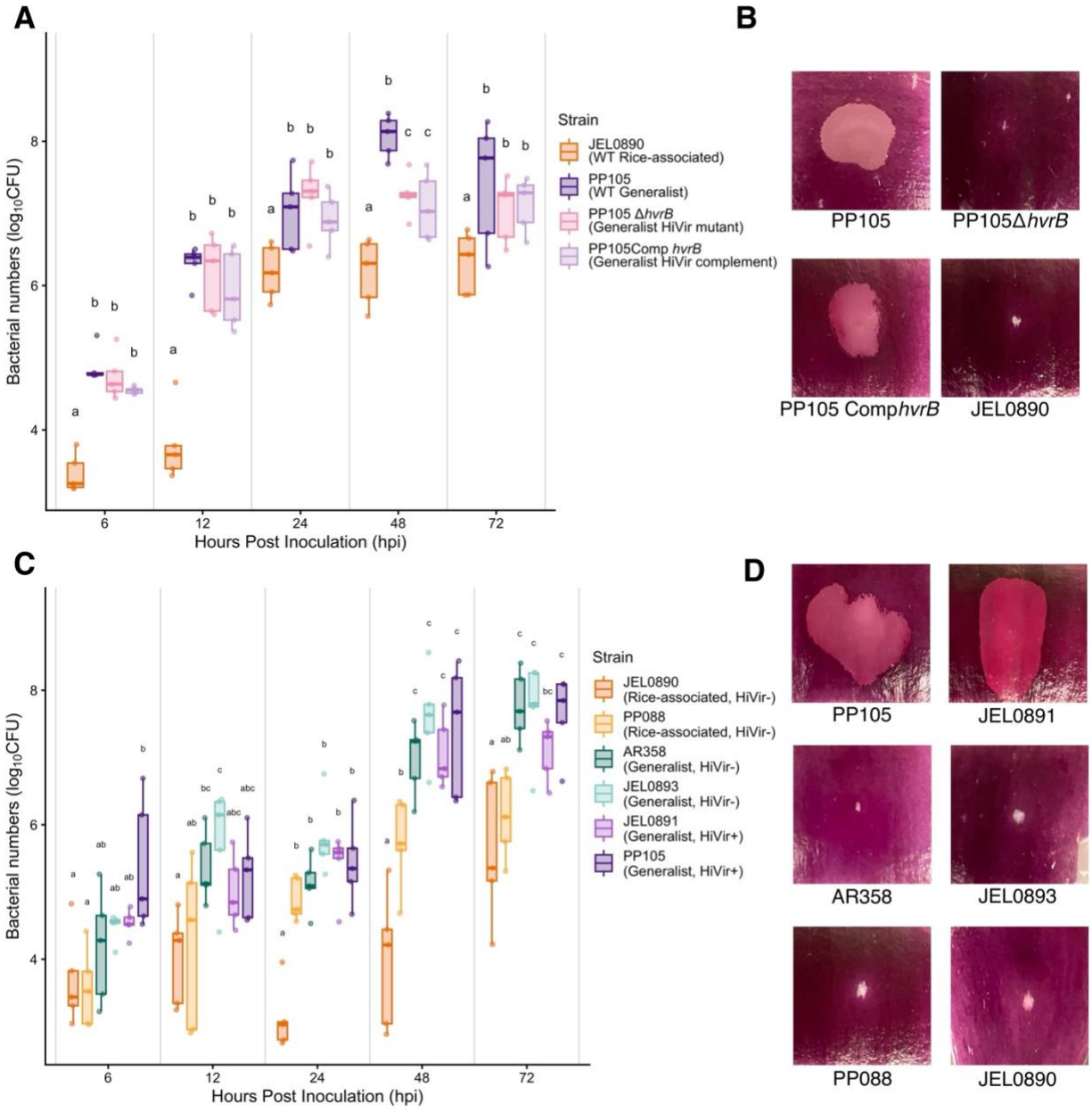


**Fig. 7.** *P. ananatis* generalist strains **A,** Time-course growth curve of generalist strains PP105, PP105Δ*hvrB*, and PP105Comp*hvrB* inoculated into red onion scales alongside rice-associated strain JEL0890. Each strain extracted from 1 cm diameter punches surrounding the infiltration site at 6, 12, 24, 48, and 72 hpi. Starting inoculum densities were 7.49, 7.39, 7.44, and 7.72 log10CFU/ml, respectively. Letters indicate statistically significant differences measured at $p < 0.05$. **B,** Symptom development of red onion scales inoculated with PP105, PP105Δ*hvrB*, and PP105Comp*hvrB*. Images taken at 72 hpi. **C,** Time-course growth curve of strains JEL0890,

PP088, AR358, JEL0893, JEL0891, and PP105 inoculated into red onion scales. Starting inoculum densities were 7.76, 7.69, 7.77, 7.58, 7.60, and 7.65 log10CFU/ml, respectively. Each strain and timepoint plated from 1cm diameter punches surrounding the infiltration site at 6, 12, 24, 48, and 72 hpi. Letters indicate statistically significant differences measured at $p < 0.05$. **D,** Symptom development of red onion scales inoculated with JEL0890, PP088, AR358, JEL0893, JEL0891, and PP105. Images taken at 72 hpi.

Allicin tolerance has been shown to play a role in *P. ananatis* replication within onion tissue (Stice et al. 2020). Strains carrying the plasmid-borne *alt* gene cluster enable the bacterium to cope with allicin, a compound released by wounded onion tissue, reaching higher bacterial levels when symptoms develop. However, HiVir-containing strains both with and without *alt* can contribute to symptom development in onion. As none of the strains we tested contain the *alt* gene cluster (Table S7), this difference in bacterial load between lineages is likely due to other strategies.

**Discussion**

Our results show that host adaptation in *P. ananatis* is structured at the lineage level, with distinct lineages differing in both genomic content and host-dependent performance. The ANI analysis resolved two major lineages with contrasting characteristics: a generalist lineage that frequently carries the HiVir operon and exhibits broad host competence, and a rice-associated lineage that lacks HiVir and is consistently recovered from rice.

A central finding of this study is that the HiVir operon is dispensable for *P. ananatis* proliferation in rice. Deletion of *hvrB* or *hvrF* did not alter *in planta* population dynamics, and strains reached similar bacterial densities over the course of infection. In contrast, HiVir had a clear effect on symptom development. HiVir-containing strains induced necrotic lesions, whereas

HiVir-deficient strains, such as those from the rice-associated lineages and the generalist mutants, did not. These data demonstrate that, in rice, necrotic symptom development driven by HiVir and bacterial proliferation within host tissue are uncoupled, indicating that virulence-associated traits do not necessarily predict pathogen performance in this host.

To our knowledge, this is the first demonstration of the decoupling of toxin-type virulence traits and bacterial proliferation in *P. ananatis,* regardless of host. However, in other systems, similar phenomena have been observed. In 1984, Turner and Taha observed indistinguishable bacterial growth during early infection of wild-type *Pseudomonas syringae* pv. *tabaci* and tabatoxin mutants inoculated in tobacco (Turner and Taha 1984), although, growth curves diverged after three dpi. Similarly, *Pseudomonas syringae* pv. *tomato* strains deficient in coronatine production were able to colonize *Arabidopsis thaliana* and tomato plants as effectively as wild-type strains, but only in salicylic acid (SA) signaling deficient plants (Brooks et al. 2005).

This separation of symptom development from bacterial multiplication contrasts with previous observations in onion, where HiVir contributes to successful colonization (Shin et al. 2023). In our experiments, strains lacking HiVir within the generalist background showed only modest differences relative to the wild-type, if any, whereas the rice-associated strain exhibited substantially reduced bacterial populations across all time points. The magnitude of this difference suggests that lineage identity, which reflects a broader genomic divergence, has a stronger influence on host colonization than HiVir status alone. Consistent with this, none of the rice-isolated strains examined carried the plasmid-borne *alt* gene cluster associated with allicin tolerance (Stice et al. 2020), indicating that additional, uncharacterized factors contribute to lineage-specific performance in onion. The fact that we were unable to reproduce increased

bacterial numbers in HiVir-containing generalists compared to HiVir-lacking generalists may be due to several factors, including the number of replicates used in our onion inoculation assays compared to previous studies.

Together, these results point to distinct evolutionary trajectories for the two lineages. Generalist strains appear to retain functions that support colonization across multiple hosts, including onion, while remaining fully competent to infect rice. In contrast, rice-associated strains exhibit reduced performance in onion, consistent with a more specialized host association. This divergence is further supported by the pangenome analysis, which identified hundreds of lineage-specific genes. We sought to functionally annotate lineage-specific genes to gain insight into divergent functions between the lineages and to pave the way for future work to identify genetic components that contribute to the host promiscuity of the generalist lineage. Interestingly, this analysis revealed substantial overlap in gene ontology, with only few exceptions. A possible explanation for this is that the two lineages achieve comparable, yet mechanistically different cellular functions through distinct gene sets, potentially reflecting divergent solutions to the ecological demands faced during host interaction. However, of note, the generalist strains contained unique genes with the COG categories of defense mechanisms and cell cycle control, cell division, chromosome partitioning, which may contribute to the observed differences in bacterial numbers during infection of certain hosts. Although the experimental characterization of these genes is lacking, their identification opens a broad set of research opportunities to uncover novel pathogenicity and virulence factors involved in plant-pathogen interactions. Additionally, as many genomes were used, differences in genome quality between the lineages may have minor impacts on inferences made from the pangenome analysis.

Nonetheless, the distribution of these genes underscores the extent of genomic differentiation between *P. ananatis* lineages.

Importantly, the ability of generalist strains to infect rice without a growth tradeoff suggests that colonization of Azucena, the rice variety tested, does not require the acquisition of specialized virulence factors. Instead, infection of Azucena may be supported by core or broadly conserved functions, while lineage-specific genes shape performance in alternative hosts. This interpretation is consistent with the observation that both lineages exhibit similar dynamics of bacterial multiplication in rice tissue despite hundreds of genes being unique to each lineage. However, it is important to note we cannot rule out the effect of rice host genotype on these observations, as this was only tested in variety Azucena.

From a practical perspective, these findings highlight that symptom severity and bacterial population size can be decoupled in this pathosystem. The presence of HiVir alters lesion development without affecting bacterial load, suggesting that visual disease symptoms may not reliably reflect pathogen abundance in rice. This has implications for both disease assessment and management.

Based on our findings, we hypothesize that disease outcomes in this pathosystem may reflect the interaction of distinct *P. ananatis* lineages with different functional capacities, rather than the behavior of a single, uniform pathogen population. Additionally, of interest is the possibility of a "division of labor" between *P. ananatis* individuals during infection of rice, as great genetic diversity exists between isolates present in the same infection court. The cooperation of distinct individuals of the same species during infection of a plant host is an emerging topic in plant pathology (Cui et al. 2019;  López-Pagán et al. 2025). Finally, future research should prioritize functional characterization of lineage-specific genes to define the

molecular basis of host specialization and generalism in *P. ananatis*. Our pangenome analysis also provides a framework for development of molecular tools that can distinguish between lineages.

**Acknowledgements**

We are deeply grateful to several people for their generous contribution to this work. We thank Brian Kvitko for providing vectors for this work and Frank White and Jose Huguet-Tapia for invaluable advice and guidance on genomic analyses. We also thank Katherine D'Amico-Willman for assisting with PacBio sequencing. We gratefully acknowledge the support of USDA-ARS Dale Bumpers National Rice Research Center. This work was supported by funding from the USDA National Plant Disease Recovery System and the Colorado State University Agricultural Experiment Station, the USDA NIFA Equipment Grants Program (2022-70410-38491) and USDA-NIFA Grant 2024-67013-42479, and the ORISE Research Participation Program, managed by Oak Ridge Associated Universities (ORAU) under DOE. Dr. Rodrigo Pedrozo was supported as an ORISE fellow through an interagency agreement between USDA ARS and the U.S. Department of Energy. USDA is an equal opportunity provider and employer. The findings and conclusions are those of the authors and do not represent the DOE, ORAU/ORISE, or official USDA or U.S. Government policy or determination.

## REFERENCES


Agarwal, G., Choudhary, D., Stice, S. P., Myers, B. K., Gitaitis, R. D., Venter, S. N., Kvitko, B. H., and Dutta, B. 2021. Pan-genome-wide analysis of *Pantoea ananatis* identified genes linked to pathogenicity in onion. Front. Microbiol. 12:684756.

Alhusays, A., Galvin, C., Torres, M., Senger, M., Fitzpatrick, E., Gonzalez-Hernandez, J. L., Glover, K., Solanki, S., and Ameen, G. 2024. First report of *Pantoea ananatis* causing leaf streak disease on wheat (*Triticum aestivum*) in the United States of America. Plant Dis. 108:2913.

Asselin, J. A. E., Bonasera, J. M., and Beer, S. V. 2016. PCR primers for detection of *Pantoea ananatis*, *Burkholderia* spp., and *Enterobacter* sp. from onion. Plant Dis. 100:836–846.

Asselin, J. A. E., Bonasera, J. M., and Beer, S. V. 2018. Center rot of onion (*Allium cepa*) caused by *Pantoea ananatis* requires *pepM*, a predicted phosphonate-related gene. Mol. Plant-Microbe Interact. 31:1291–1300.

Azad, H., Holmes, G., and Cooksey, D. 2000. A new leaf blotch disease of sudangrass caused by *Pantoea ananas* and *Pantoea stewartii*. Plant Dis. 84:973–979.

Azizi, M. M. F., Ismail, S. I., Ina-Salwany, M. Y., Hata, E. M., and Zulperi, D. 2020. The emergence of *Pantoea* species as a future threat to global rice production. J. Plant Prot. Res.:327–335.

Bing, X.-L., Wan, Y.-Y., Liu, H.-H., Ji, R., Zhao, D.-S., Niu, Y.-D., Li, T.-P., and Hong, X.-Y. 2022. Characterization of *Pantoea ananatis* from rice planthoppers reveals a clade of rice-associated *P. ananatis* undergoing genome reduction. Microb. Genom. 8:000907.

Bouras, G., Sheppard, A. E., Mallawaarachchi, V., and Vreugde, S. 2023. Plassembler: an automated bacterial plasmid assembly tool. Bioinformatics 39:btad409.

Bouras, G., Grigson, S. R., Papudeshi, B., Mallawaarachchi, V., and Roach, M. 2024. Dnaapler: a tool to reorient circular microbial genomes. J. Open Source Softw. 9:5968.

Brooks, D. M., Bender, C. L., and Kunkel, B. N. 2005. The *Pseudomonas syringae* phytotoxin coronatine promotes virulence by overcoming salicylic acid-dependent defences in *Arabidopsis thaliana*. Mol. Plant Pathol. 6:629–639.

Bruno, J., Barphagha, I., Ontoy, J., Dalla Lana, F., and Ham, J. H. 2025. First report of *Pantoea ananatis* causing bacterial leaf and panicle blight of rice in Louisiana, USA. Plant Dis. 109:932.

Brynildsrud, O., Bohlin, J., Scheffer, L., and Eldholm, V. 2016. Rapid scoring of genes in microbial pan-genome-wide association studies with Scoary. Genome Biol. 17:238.

Buchfink, B., Xie, C., and Huson, D. H. 2015. Fast and sensitive protein alignment using DIAMOND. Nat. Methods 12:59–60.

Cantalapiedra, C. P., Hernández-Plaza, A., Letunic, I., Bork, P., and Huerta-Cepas, J. 2021. eggNOG-mapper v2: functional annotation, orthology assignments, and domain prediction at the metagenomic scale. Mol. Biol. Evol. 38:5825–5829.

Chathalingath, N., and Gunasekar, A. 2023. First report of *Pantoea ananatis* causing leaf blight disease of pomegranate in India. New Dis. Rep. 48:e12233.

Chen, S., Zhou, Y., Chen, Y., and Gu, J. 2018. fastp: an ultra-fast all-in-one FASTQ preprocessor. Bioinformatics 34:i884–i890.

Cheng, H., Concepcion, G. T., Feng, X., Zhang, H., and Li, H. 2021. Haplotype-resolved de novo assembly using phased assembly graphs with hifiasm. Nat. Methods 18:170–175.

Cota, L., Costa, R., Silva, D., Parreira, D., Lana, U., and Casela, C. 2010. First report of pathogenicity of *Pantoea ananatis* in sorghum (*Sorghum bicolor*) in Brazil. Australas. Plant Dis. Notes 5:120–122.

Coutinho, T. A., and Venter, S. N. 2009. *Pantoea ananatis*: an unconventional plant pathogen. Mol. Plant Pathol. 10:325–335.

Coutinho, T. A., Preisig, O., Mergaert, J., Cnockaert, M. C., Riedel, K. H., Swings, J., and Wingfield, M. J. 2002. Bacterial blight and dieback of eucalyptus species, hybrids, and clones in South Africa. Plant Dis. 86:20–25.

Cui, Z., Yang, C.-H., Kharadi, R. R., Yuan, X., Sundin, G. W., Triplett, L. R., Wang, J., and Zeng, Q. 2019. Cell-length heterogeneity: a population-level solution to growth/virulence trade-offs in the plant pathogen *Dickeya dadantii*. PLoS Pathog. 15:e1007703.

Danecek, P., Bonfield, J. K., Liddle, J., Marshall, J., Ohan, V., Pollard, M. O., Whitwham, A., Keane, T., McCarthy, S. A., and Davies, R. M. 2021. Twelve years of SAMtools and BCFtools. Gigascience 10:giab008.

Das, A., Kumar, A., Nerkar, S., Chichghare, S., and Pali, P. 2020. First report of *Pantoea ananatis* causing fruitlet blight of Nagpur mandarin (*Citrus reticulata*) in India. New Dis. Rep. 41:5–5.

De Maayer, P., Chan, W. Y., Rubagotti, E., Venter, S. N., Toth, I. K., Birch, P. R., and Coutinho, T. A. 2014. Analysis of the *Pantoea ananatis* pan-genome reveals factors underlying its ability to colonize and interact with plant, insect and vertebrate hosts. BMC Genom. 15:1–14.

De Maayer, P., Aliyu, H., Vikram, S., Blom, J., Duffy, B., Cowan, D. A., Smits, T. H., Venter, S. N., and Coutinho, T. A. 2017. Phylogenomic, pan-genomic, pathogenomic and evolutionary genomic insights into the agronomically relevant enterobacteria *Pantoea ananatis* and *Pantoea stewartii*. Front. Microbiol. 8:1755.

de Paula, S., Belmar, S., Giebler, M., Ferreira, A. C., Ronning, B., Jia, Y., Pedrozo, R., Leach, J. E., Luna, E., and Nicolli, C. 2026. Unraveling the Dynamics of *Pantoea ananatis*: Isolation and Plant Responses. Phytopathology.

Galaxy, C. 2024. The Galaxy platform for accessible, reproducible, and collaborative data analyses: 2024 update. Nucleic Acids Research 52:W83–W94.

Gao, F., Liu, Z., Anane, R. F., Li, S., Zhou, W., Zi, S., Chu, B., Liu, J., Chen, X., and Chen, Z. 2024. First report of *Pantoea ananatis* causing leaf spot disease in tobacco (*Nicotiana tabacum*) in China. Plant Dis. 108:2214.

Gavini, F., Mergaert, J., Beji, A., Mielcarek, C., Izard, D., Kersters, K., and De Ley, J. 1989. Transfer of *Enterobacter agglomerans* (Beijerinck 1888) Ewing and Fife 1972 to *Pantoea* gen. nov. as *Pantoea agglomerans* comb, nov. and description of *Pantoea dispersa* sp. nov. Int. J. Syst. Evol. Microbiol. 39:337–345.

Gilchrist, C. L. M., Booth, T. J., van Wersch, B., van Grieken, L., Medema, M. H., and Chooi, Y. H. 2021. cblaster: a remote search tool for rapid identification and visualization of homologous gene clusters. Bioinform. Adv. 1:vbab016.

Gitaitis, R., and Gay, J. 1997. First report of a leaf blight, seed stalk rot, and bulb decay of onion by *Pantoea ananas* in Georgia. Plant Dis. 81:1096–1096.

Gitaitis, R., Walcott, R., Culpepper, S., Sanders, H., Zolobowska, L., and Langston, D. 2002. Recovery of *Pantoea ananatis*, causal agent of center rot of onion, from weeds and crops in Georgia, USA. Crop Prot. 21:983–989.

Goszczynska, T., Botha, W., Venter, S., and Coutinho, T. 2007. Isolation and identification of the causal agent of brown stalk rot, a new disease of maize in South Africa. Plant Dis. 91:711–718.

Gutiérrez-Barranquero, J. A., Cazorla, F., Torés, J. A., and De Vicente, A. 2019. First report of *Pantoea ananatis* causing necrotic symptoms in mango trees in the Canary Islands, Spain. Plant Dis. 103:1017.

Hall, M. B., Zhou, C., and Coin, L. J. 2025. Genome size estimation from long read overlaps. Bioinformatics 41:btaf593.

Kido, K., Adachi, R., Hasegawa, M., Yano, K., Hikichi, Y., Takeuchi, S., Atsuchi, T., and Takikawa, Y. 2008. Internal fruit rot of netted melon caused by *Pantoea ananatis* (= *Erwinia ananas*) in Japan. J. Gen. Plant Pathol. 74:302–312.

Kim, H. J., Lee, J. H., Kang, B. R., Rong, X., McSpadden Gardener, B. B., Ji, H. J., Park, C. S., and Kim, Y. C. 2012. Draft genome sequence of *Pantoea ananatis* B1-9, a nonpathogenic plant growth-promoting bacterium. J. Bacteriol. 194:729.

Kolmogorov, M., Yuan, J., Lin, Y., and Pevzner, P. A. 2019. Assembly of long, error-prone reads using repeat graphs. Nat. Biotechnol. 37:540–546.

Krawczyk, K., Wielkopolan, B., and Obrępalska-Stęplowska, A. 2020. *Pantoea ananatis*, a new bacterial pathogen affecting wheat plants (*Triticum* L.) in Poland. Pathogens 9:1079.

LaGier, M. J., McDaniel, M., Ragner, A., and Castillo, A. 2022. Identification and characterization of a potential antibiotic producing strain of *Pantoea ananatis*. J. Genom. 10:26.

Lao, G., Jin, P., Miao, W., and Liu, W. 2023. First report of leaf spot on cucumber caused by *Pantoea ananatis* in Hainan, China. Plant Dis. 107:1214.

Li, H. 2016. Minimap and miniasm: fast mapping and de novo assembly for noisy long sequences. Bioinformatics 32:2103–2110.

Liao, L., Hei, R., Tang, Y., Liu, S., and Zhou, J. 2016. First report of soft rot disease of peach caused by *Pantoea ananatis* in China. Plant Dis. 100:516–516.

López-Pagán, N., Rufián, J. S., Luneau, J., Sánchez-Romero, M.-A., Aussel, L., van Vliet, S., Ruiz-Albert, J., and Beuzón, C. R. 2025. *Pseudomonas syringae* subpopulations cooperate by coordinating flagellar and type III secretion spatiotemporal dynamics to facilitate plant infection. Nat. Microbiol. 10:958–972.

Luhung, I., Junqueira, A., Uchida, A., Purbojati, R., Houghton, J., Chénard, C., Wong, A., Clare, M., Kushwaha, K., and Panicker, D. 2018. Genome sequence of *Pantoea ananatis* SGAir0210, isolated from outdoor air in Singapore. Genome Announc.:e00643–00618.

Luna, E., Lang, J., McClung, A., Wamishe, Y., Jia, Y., and Leach, J. E. 2023. First report of rice bacterial leaf blight disease caused by *Pantoea ananatis* in the United States. Plant Dis. 107:2214.

Mano, H., Tanaka, F., Watanabe, A., Kaga, H., Okunishi, S., and Morisaki, H. 2006. Culturable surface and endophytic bacterial flora of the maturing seeds of rice plants (*Oryza sativa*) cultivated in a paddy field. Microbes Environ. 21:86–100.

Megías, E., Megías, M., Ollero, F. J., and Hungria, M. 2016. Draft genome sequence of *Pantoea ananatis* strain AMG521, a rice plant growth-promoting bacterial endophyte isolated from the Guadalquivir marshes in southern Spain. Genome Announc. 4:10–1128.

Mergaert, J., Verdonck, L., and Kersters, K. 1993. Transfer of *Erwinia ananas* (synonym, *Erwinia uredovora*) and *Erwinia stewartii* to the genus *Pantoea* emend. as *Pantoea ananas* (Serrano 1928) comb. nov. and *Pantoea stewartii* (Smith 1898) comb. nov.,

respectively, and description of *Pantoea stewartii* subsp. *indologenes* subsp. nov. Int. J. Syst. Evol. Microbiol. 43:162–173.
Mondal, K., Mani, C., Singh, J., Kim, J.-G., and Mudgett, M. 2011. A new leaf blight of rice caused by *Pantoea ananatis* in India. Plant Dis. 95:1582–1582.
Morohoshi, T., Nakamura, Y., Yamazaki, G., Ishida, A., Kato, N., and Ikeda, T. 2007. The plant pathogen *Pantoea ananatis* produces N-acylhomoserine lactone and causes center rot disease of onion by quorum sensing. J. Bacteriol. 189:8333–8338.
Obasa, K., Coker, D., and Santiago-Gonzalez, J. 2024. Late-season decline, a bacterial disease of corn caused by *Pantoea ananatis*, identified in sorghum. Plant Health Prog. 25:348–352.
Obasa, K., Kolomiets, M., Reed, B., Coker, D., Bell, J., and Heflin, K. 2023. Late-season decline: A new bacterial disease of corn identified in the Texas panhandle. Plant Health Prog. 24:198–206.
Okunishi, S., Sako, K., Mano, H., Imamura, A., and Morisaki, H. 2005. Bacterial flora of endophytes in the maturing seed of cultivated rice (*Oryza sativa*). Microbes Environ. 20:168–177.
Page, A. J., Cummins, C. A., Hunt, M., Wong, V. K., Reuter, S., Holden, M. T., Fookes, M., Falush, D., Keane, J. A., and Parkhill, J. 2015. Roary: rapid large-scale prokaryote pan genome analysis. Bioinformatics 31:3691–3693.
Parks, D. H., Imelfort, M., Skennerton, C. T., Hugenholtz, P., and Tyson, G. W. 2015. CheckM: assessing the quality of microbial genomes recovered from isolates, single cells, and metagenomes. Genome Res. 25:1043.
Polidore, A. L., Caserio, A. D., Zhu, L., and Metcalf, W. W. 2024. Complete biochemical characterization of pantaphos biosynthesis highlights an unusual role for a SAM-dependent methyltransferase. Angew. Chem. Int. Ed. 63:e202317262.
Polidore, A. L. A., Furiassi, L., Hergenrother, P. J., and Metcalf, W. W. 2021. A phosphonate natural product made by *Pantoea ananatis* is necessary and sufficient for the hallmark lesions of onion center rot. Mbio 12:10.1128.
Pritchard, L., Glover, R. H., Humphris, S., Elphinstone, J. G., and Toth, I. K. 2016. Genomics and taxonomy in diagnostics for food security: soft-rotting enterobacterial plant pathogens. Anal. Methods 8:12–24.
Rauch, M. E., Graef, H. W., Rozenzhak, S. M., Jones, S. E., Bleckmann, C. A., Kruger, R. L., Naik, R. R., and Stone, M. O. 2006. Characterization of microbial contamination in United States Air Force aviation fuel tanks. J. Ind. Microbiol. Biotechnol. 33:29–36.
Reimers, P., and Leach, J. 1991. Race-specific resistance to *Xanthomonas oryzae* pv. *oryzae* conferred by bacterial blight resistance gene Xa-10 in rice (*Oryza sativa*) involves accumulation of a lignin-like substance in host tissues. Physiol. Mol. Plant Pathol. 38:39–55.
Schwartz, H., and Otto, K. 2000. First report of a leaf blight and bulb decay of onion by *Pantoea ananitas* in Colorado. Plant Dis. 84:808–808.
Schwengers, O., Jelonek, L., Dieckmann, M. A., Beyvers, S., Blom, J., and Goesmann, A. 2021. Bakta: rapid and standardized annotation of bacterial genomes via alignment-free sequence identification. Microb. Genom. 7:000685.
Serrano, F. 1928. Bacterial fruitlet brown-rot of pineapple in the Philippines. The Philippine Journal of Science 36:271–305.
Sheibani-Tezerji, R., Naveed, M., Jehl, M.-A., Sessitsch, A., Rattei, T., and Mitter, B. 2015. The genomes of closely related *Pantoea ananatis* maize seed endophytes having different

effects on the host plant differ in secretion system genes and mobile genetic elements. Front. Microbiol. 6:440.
Shin, G. Y., Dutta, B., and Kvitko, B. 2023. The genetic requirements for HiVir-mediated onion necrosis by *Pantoea ananatis*, a necrotrophic plant pathogen. Mol. Plant-Microbe Interact. 36:381–391.
Shin, G. Y., Smith, A., Coutinho, T. A., Dutta, B., and Kvitko, B. H. 2022. Validation of species-specific PCR assays for the detection of *Pantoea ananatis, P. agglomerans, P. allii*, and *P. stewartii*. Plant Dis. 106:2563–2570.
Sibanda, S., Theron, J., Shyntum, D. Y., Moleleki, L. N., and Coutinho, T. A. 2016. Characterization of two LuxI/R homologs in *Pantoea ananatis* LMG 2665T. Can. J. Microbiol. 62:893–903.
Stice, S. P., Stumpf, S. D., Gitaitis, R. D., Kvitko, B. H., and Dutta, B. 2018. *Pantoea ananatis* genetic diversity analysis reveals limited genomic diversity as well as accessory genes correlated with onion pathogenicity. Front. Microbiol. 9:184.
Stice, S. P., Thao, K. K., Khang, C. H., Baltrus, D. A., Dutta, B., and Kvitko, B. H. 2020. Thiosulfinate tolerance is a virulence strategy of an atypical bacterial pathogen of onion. Curr. Biol. 30:3130–3140.
Stice, S. P., Shin, G. Y., De Armas, S., Koirala, S., Galván, G. A., Siri, M. I., Severns, P. M., Coutinho, T., Dutta, B., and Kvitko, B. H. 2021. The distribution of onion virulence gene clusters among *Pantoea* spp. Front. Plant Sci. 12:643787.
Turner, J., and Taha, R. 1984. Contribution of tabtoxin to the pathogenicity of *Pseudomonas syringae* pv. *tabaci*. Physiol. Plant Pathol. 25:55–69.
Vaser, R., and Šikić, M. 2021. Time-and memory-efficient genome assembly with Raven. Nat. Comput. Sci. 1:332–336.
Vasimuddin, M., Misra, S., Li, H., and Aluru, S. 2019. Efficient architecture-aware acceleration of BWA-MEM for multicore systems. Pages 314–324 in: 2019 IEEE international parallel and distributed processing symposium (IPDPS) IEEE.
Wang, D. R., Jamshidi, S., Han, R., Edwards, J. D., McClung, A. M., and McCouch, S. R. 2024. Positive effects of public breeding on US rice yields under future climate scenarios. Proc. Natl. Acad. Sci. USA 121:e2309969121.
Wang, M., Ma, J., Xu, Z., Feng, X., and Xu, H. 2019. First report of shoot blight on fragrant pear caused by *Pantoea ananatis* in China. Plant Dis. 103:1764–1764.
Watanabe, K., Kawakita, H., and Sato, M. 1996. Epiphytic bacterium, *Erwinia ananas*, commonly isolated from rice plants and brown planthoppers (*Nilaparvata lugens*) in hopperburn patches. Appl. Entomol. Zool. 31:459–462.
Weller-Stuart, T., De Maayer, P., and Coutinho, T. 2017a. *Pantoea ananatis*: genomic insights into a versatile pathogen. Mol. Plant Pathol. 18:1191–1198.
Weller-Stuart, T., Toth, I., De Maayer, P., and Coutinho, T. 2017b. Swimming and twitching motility are essential for attachment and virulence of *Pantoea ananatis* in onion seedlings. Mol. Plant Pathol. 18:734–745.
Wick, R. R., and Holt, K. E. 2022. Polypolish: short-read polishing of long-read bacterial genome assemblies. PLoS Comput. Biol. 18:e1009802.
Wick, R. R., Howden, B. P., and Stinear, T. P. 2025. Autocycler: long-read consensus assembly for bacterial genomes. Bioinformatics 41:btaf474.

Wick, R. R., Judd, L. M., Cerdeira, L. T., Hawkey, J., Méric, G., Vezina, B., Wyres, K. L., and Holt, K. E. 2021. Trycycler: consensus long-read assemblies for bacterial genomes. Genome Biol. 22:266.

Yan, H., Yu, S., Xie, G.-L., Fang, W., Su, T., and Li, B. 2010. Grain discoloration of rice caused by *Pantoea ananatis* (synonym *Erwinia uredovora*) in China. Plant Dis. 94:482–482.

Yuan, T., Huang, Y., Luo, L., Wang, J., Li, J., Chen, J., Qin, Y., and Liu, J. 2023. Complete genome sequence of *Pantoea ananatis* strain LCFJ-001 isolated from bacterial wilt mulberry. Plant Dis. 107:2500–2505.

Zhang, Y., Zheng, L., Gao, H., Song, Q., and Gao, J. 2019. First report of a new bacterial leaf blight of Chinese cabbage (*Brassica rapa pekinensis*) caused by *Pantoea ananatis* in China. Plant Dis. 103:2942.

Zhao, X., Gao, L., Huang, H., Zhao, Y., Hanif, A., Wu, H., Gu, Q., Wu, L., and Gao, X. 2021. Exploring the pathogenic function of *Pantoea ananatis* endogenous plasmid by an efficient and simple plasmid elimination strategy. Microbiol. Res. 246:126710.

Zhao, X., Gao, L., Ali, Q., Yu, C., Yuan, B., Huang, H., Long, J., Gu, Q., Wu, H., and Gao, X. 2024. A type VI secretion system effector TseG of *Pantoea ananatis* is involved in virulence and antibacterial activity. Mol. Plant Pathol. 25:e13442.

# APPENDIX I: ADDITIONAL GENOMIC ANALYSES OF RICE-ISOALTED *PANTOEA ANANATIS*

## Introduction

In the genomics era, whole genome sequencing has led to an eruption of insight into plant pathogenic bacteria. Researchers can investigate the origins of certain microbes, gaining knowledge of the pathosystems from which they emerged, and learn how our management actions, environmental conditions, and host defenses have influenced their evolution. Importantly, available genomes have uncovered the genetic basis of virulence for many phytopathogens, enabling more effective management strategies and saving producers from enormous losses (Koebnik et al. 2024; Straub et al. 2021).

In fact, some of the most significant discoveries in plant pathology have come since the unveiling of whole genome sequencing technologies. Sequencing of *Xanthomonas* genomes led to an understanding of the DNA binding activity of transcription activator-like effectors (TALEs), opening the door to targeted gene editing to disrupt their interactions (Koebnik et al. 2024). Beyond a phytopathological perspective, this enabled the invention of TALENs (TALE nucleases) which are widely used in gene editing (Koebnik et al. 2024). Additionally, genome-wide association studies (GWAS), traditionally used in plant and human genetics, have been used to identify bacterial genomic variants associated with specific traits of interest, namely virulence (Straub et al. 2021).

Despite recent advances, the need for genomic analyses of plant pathogenic bacteria is still ever present, as pathogen populations constantly shift and evolve to overcome plant defenses and human management strategies (Straub et al. 2021; Timilsina et al. 2022). Because bacteria

frequently exchange genetic elements, novel genes encoding important virulence factors can suddenly enable pathogenic capability and facilitate host range expansion (Maddock and Hulin 2025). Alternatively, sudden mutations of certain effectors or pathogen-associated molecular patterns (PAMPs) enable pathogens to evade host defense systems of previously resistant crops (Ogbuji and Agogbua 2025).

In order to gain better insight into the emerging epidemic of *P. ananatis* on rice, several genomic analyses on the twelve strains sequenced in Chapter 2 were performed to characterize factors potentially contributing to pathogenic interactions with rice hosts. A focus was placed on secretion system characterization and identification of secondary metabolite production potential from strains isolated from rice. As previously demonstrated, rice-isolated *P. ananatis* is structured into two distinct lineages, one containing strains with strict rice host associations, and a generalist lineage, containing strains with more host promiscuity. These additional genomic analyses were performed with this in mind.

## Methods

### Genome annotation

Genome assemblies of the twelve genomes sequenced in chapter 2 were annotated using Bakta v1.9.3 (Schwengers et al. 2021) via Galaxy platform v1.9.4 (Galaxy 2024) for annotation of protein coding sequences, tRNAs, rRNAs, and non-coding RNAs.

### Secretion system characterization

Protein FASTA files from Bakta were submitted to TXSScan v1.0.3, hosted on Galaxy Pasteur v1.0.3 (Mareuil et al. 2017), a program that uses MacSyFinder software v2.1.3 (Néron et

al. 2023) for secretion system prediction. TXSScan employs Hidden Markov Models (HMMs) to identify components of Types I through VI secretion systems.

As Type VI secretion systems (T6SS) have been shown to play a pivotal role for *P. ananatis* pathogenesis in some systems (De Maayer et al. 2014; Zhao et al. 2024), putative T6SS clusters were extracted from the genomes and compared to three known T6SS of *P. ananatis* strain LMG20103 (GenBank accession SAMN02603236) using BLASTp with default parameters.

Putative Type III secretion system (T3SS) clusters identified by TXSScan were extracted from the genomes and compared to the *P. stewartii* subsp. *stewartii* T3SS repertoire (PSI-1, PSI-2, and PSI-3 systems) (Correa et al. 2012). using BLASTp with default parameters.

**Secondary metabolite characterization**

Genome annotations were uploaded to antiSMASH v8.0 (Blin et al. 2025) web server (https://antismash.secondarymetabolites.org/) to identify biosynthetic gene clusters (BGCs) for secondary metabolites. antiSMASH uses HMMs and comparative genomics to detect, annotate, and analyze secondary metabolite biosynthetic gene clusters in microbial genomes. Relaxed detection strictness settings were used to maximize BGC discovery.

## Results

**Secretion system distribution**

All *P. ananatis* strains sequenced in this study contained Type I (T1SS), Type V (T5SS), and Type VI (T6SS) secretion systems, consistent with previous reports of their conservation within the species (De Maayer et al. 2017). They also contain a Type IV pilus (T4aP) system for

motility (Weller-Stuart et al. 2017). Among T6SS clusters identified, all strains contained T6SS-1 and T6SS-3, both of which are also conserved among the species (De Maayer et al. 2017; Shyntum et al. 2014). A sporadic distribution of T6SS-2 was observed, consistent with previous reports (De Maayer et al. 2017; Shyntum et al. 2014), with four matches to the rice-associated lineage (strains JEL0889, JEL0890, PP088, and PP092). A single generalist strain was predicted to encode T6SS-2 (strain JEL0893). In all genomes with T6SS-2, five genes were absent compared to LMG20103, although they are not part of the core T6SS and are unlikely to have essential contribution to T6SS function (De Maayer et al. 2017).

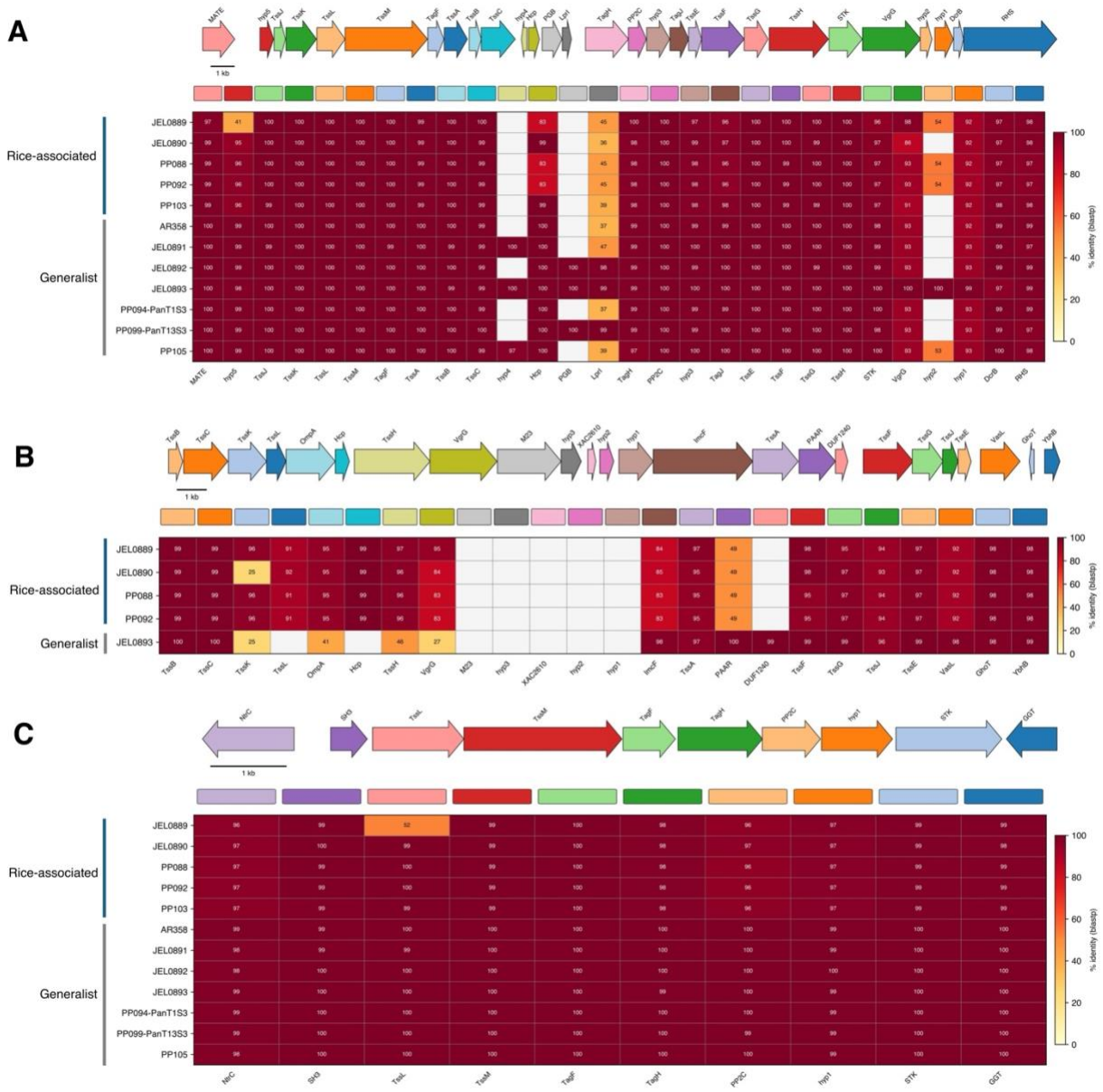


**Fig. 1.** Identification of T6SS in twelve rice-isolated *P. ananatis* genomes. Protein homology based on blastp results compared T6SS sequences found in *P. ananatis* strain LMG20103. **A,** T6SS-1. **B,** T6SS-2. **C,** T6SS-3.

Five of the strains encoded a T3SS, with high homology to the *P. stewartii* subsp. *stewartii* PSI-2 system. Again, this distribution contained four strains from the rice-associated lineage (JEL0889, PP088, PP092, and PP103) and one strain from the generalist lineage

(JEL0893). PSI-1 and PSI-3 were not detected in *P. ananatis* genomes. All TXSScan T3SS hits were identified as PSI-2.

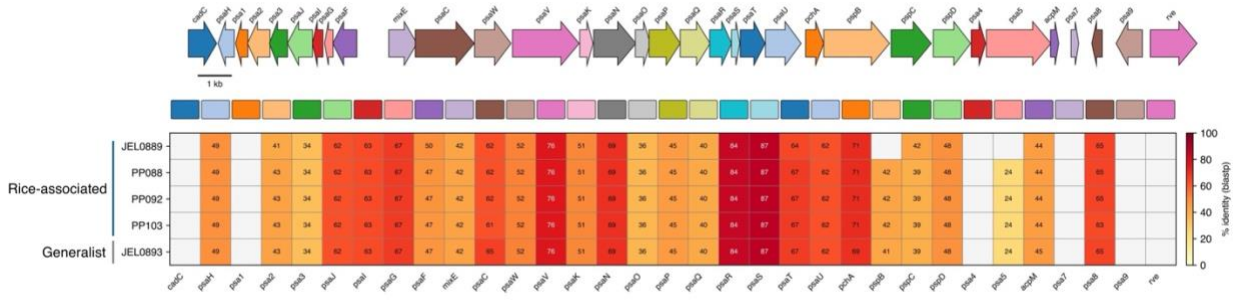


**Fig. 2.** Identification of T3SS PSI-2 in five of twelve rice-isolated *P. ananatis* genomes. Protein homology based on blastp results compared T3SS sequences found in *P. stewartii* subsp. *stewartii* strain DC283.

## Secondary Metabolite Profiles

Using antiSMASH, a diverse array of putative secondary metabolites were identified across the twelve genomes. In five of the twelve genomes, phosphonate biosynthesis was predicted, and the identity of the biosynthetic gene cluster match was that of HiVir (Polidore et al. 2024; Polidore et al. 2021; Shin et al. 2023). This BGC was only present in generalist strains (JEL0891, JEL0892, PP094-PanT1S3, PP099-PanT13S3, and PP105) and confirmed PCR results from chapter 2.

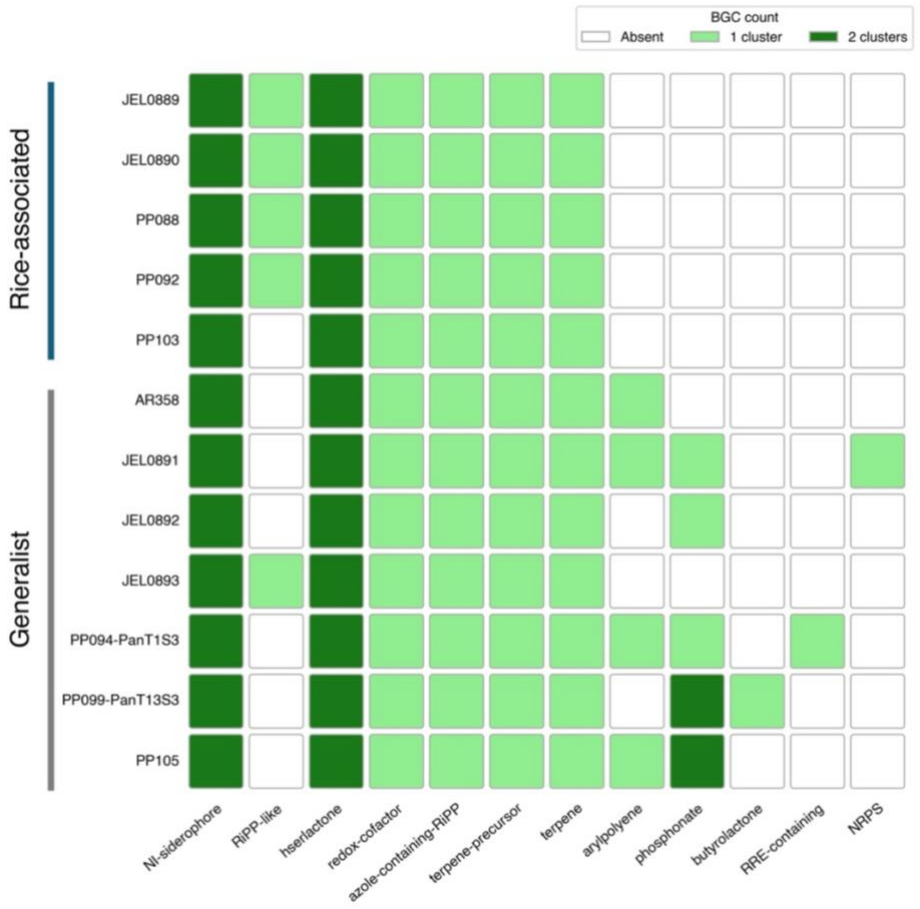


**Fig. 3.** Distribution of predicted secondary metabolite biosynthetic gene clusters present in twelve rice-isolated *P. ananatis* strains. Dark green represents two hits identified, light green represents one hit identified, and white indicates no cluster found.

Intriguingly, two other secondary metabolites displayed uneven distribution between the rice-associated and generalist lineages. A predicted arylpolyene-type biosynthetic gene cluster was observed in four of the seven generalist lineage strains (AR358, JEL0891, PP094-PanT1S3, and PP105) and was absent from all rice-associated strains.

Conversely, a RiPP-like (ribosomally synthesized and post-translationally modified peptide) biosynthetic gene cluster was identified in four of five rice-associated strains (JEL0889, JEL0890, PP088, and PP092) and only one of the seven generalist strains (JEL0893). Overall,

the rice-associated lineage contained a more constrained secondary metabolite profile than the generalist lineage.

## Discussion

The genomic analyses of secretion systems and secondary metabolites in rice-isolated *P. ananatis* strains revealed distinct patterns that correlate with the previously identified phylogenetic structure. The presence of T6SS-2 and T3SS PSI-2 predominantly in the rice-associated lineage suggests these systems may play important roles during infection of rice. The T6SS is known to be involved in host interactions with maize, potato, and onion (Zhao et al. 2024), while T3SS PSI-2 is directly involved in interactions with insect hosts in *P. stewartii* subsp. *stewartii.* The role that PSI-2 has in *P. ananatis* remains to be discovered.

Also of interest is the observed distribution of two BGCs encoding an arylpolyene and a RiPP-like compound. Arylpolyenes are a highly abundant and widespread across bacteria, and are structurally and functionally analogous to antioxidative carotenoids (Schöner et al. 2016). To date, their characterized biological function is primarily associated with protection from oxidative and photooxidative stress as they are capable of scavenging reactive oxygen species (ROS) (Schöner et al. 2016). When produced by Gram-negative bacteria, they are associated with the formation of thicker and denser biofilms (Johnston et al. 2021). In plant-microbe interactions, they have been shown to enhance microbial fitness on the surface of leaves, where bacteria typically experienced more intense sunlight and UV exposure (He et al. 2020). Once inside of the plant, arylpolyenes may aid in the ability to tolerate ROS produced by the infected plant (He et al. 2020).

The identification of an arylpolyene BGC associated with the generalist strains of *P. ananatis* is particularly interesting, as this group of the species is typically associated with distinct, HiVir-mediated symptom development on host plants, and while it has not been shown directly, the possibility remains that plants infected with generalist strains may produce more ROS in response to toxin production.

Ribosomally synthesized and post-translationally modified peptides (RiPPs), a type of metabolite that also displayed uneven distribution among the *P. ananatis* lineages, are a diverse family of natural products. They are primarily produced by bacteria, but are present across all three domains of life (Arnison et al. 2013). All RiPP-like BGCs share some commonalities that include at least one precursor peptide and one to several post-translational modification enzymes (Li and Rebuffat 2020). In bacteria, the characterization of RiPPs have revealed that they often act as antimicrobial compounds such as bacteriocins (Li and Rebuffat 2020), but their functional role extends far beyond this, acting as autoinducing signaling molecules, enzyme cofactors, and mediators of host-microbe interactions (Li and Rebuffat 2020). They have also been shown to play an important role in metal stress tolerance (Leprevost et al. 2024).

In the context of plant pathology, a well characterized RiPP produced by *Xanthomonas oryzae* pv. *oryzae* (*Xoo*), RaxX, is important for rice-host interactions (Luu et al. 2019). RaxX structurally mimics the endogenous plant peptide hormone PSY1 (Pruitt et al. 2017; Pruitt et al. 2015). PSY1 is normally utilized to promote cellular proliferation and expansion, but RaxX is utilized to mimic and reprogram the host's cellular environment and support infection (Pruitt et al. 2017). Resistant varieties have evolved a specific immune receptor, XA21, as a counter-defense mechanism. XA21 binds to the RaxX peptide but ignores the plant's endogenous PSY1

hormone. Upon recognition of RaxX, XA21 triggers a robust innate immune response to *Xoo* (Luu et al. 2019; Pruitt et al. 2017; Pruitt et al. 2015).

The identification of a RiPP-like BGC, enriched in the rice-associated *P. ananatis* lineage, warrants further investigation due to its potential to influence host-microbe interactions. However, because RiPPs possess extremely diverse properties, functional characterization of this *P. ananatis* RiPP will be needed to understand if its role, if any, during infection of rice.

Overall, these findings contribute to our understanding of the evolutionary dynamics of *P. ananatis* and highlight the importance of genomic approaches in characterizing emerging plant pathogen populations. The correlation between phylogenetic structure and gene content provides evidence for ongoing specialization within *P. ananatis* populations. Furthermore, the genomic characterization presented here provides a foundation for future investigations into the molecular mechanisms underlying host specialization for *P. ananatis.* Understanding these evolutionary adaptations will be crucial for development of targeted management strategies and for the understanding of host specialization in other bacterial systems.

## REFERENCES


Arnison, P. G., Bibb, M. J., Bierbaum, G., Bowers, A. A., Bugni, T. S., Bulaj, G., Camarero, J. A., Campopiano, D. J., Challis, G. L., and Clardy, J. 2013. Ribosomally synthesized and post-translationally modified peptide natural products: overview and recommendations for a universal nomenclature. Nat. Prod. Rep. 30:108–160.

Blin, K., Shaw, S., Vader, L., Szenei, J., Reitz, Z. L., Augustijn, H. E., Cediel-Becerra, J. D., de Crécy-Lagard, V., Koetsier, R. A., and Williams, S. E. 2025. antiSMASH 8.0: extended gene cluster detection capabilities and analyses of chemistry, enzymology, and regulation. Nucleic Acids Research 53:W32–W38.

Correa, V. R., Majerczak, D. R., Ammar, E.-D., Merighi, M., Pratt, R. C., Hogenhout, S. A., Coplin, D. L., and Redinbaugh, M. G. 2012. The bacterium *Pantoea stewartii* uses two different type III secretion systems to colonize its plant host and insect vector. Appl. Environ. Microbiol. 78:6327–6336.

De Maayer, P., Chan, W. Y., Rubagotti, E., Venter, S. N., Toth, I. K., Birch, P. R., and Coutinho, T. A. 2014. Analysis of the *Pantoea ananatis* pan-genome reveals factors underlying its ability to colonize and interact with plant, insect and vertebrate hosts. BMC Genom. 15:1–14.

De Maayer, P., Aliyu, H., Vikram, S., Blom, J., Duffy, B., Cowan, D. A., Smits, T. H., Venter, S. N., and Coutinho, T. A. 2017. Phylogenomic, pan-genomic, pathogenomic and evolutionary genomic insights into the agronomically relevant enterobacteria *Pantoea ananatis* and *Pantoea stewartii*. Front. Microbiol. 8:1755.

Galaxy, C. 2024. The Galaxy platform for accessible, reproducible, and collaborative data analyses: 2024 update. Nucleic Acids Research 52:W83–W94.

He, Y.-W., Cao, X.-Q., and Poplawsky, A. R. 2020. Chemical structure, biological roles, biosynthesis and regulation of the yellow xanthomonadin pigments in the phytopathogenic genus *Xanthomonas*. Mol. Plant-Microbe Interact. 33:705–714.

Johnston, I., Osborn, L. J., Markley, R. L., McManus, E. A., Kadam, A., Schultz, K. B., Nagajothi, N., Ahern, P. P., Brown, J. M., and Claesen, J. 2021. Identification of essential genes for *Escherichia coli* aryl polyene biosynthesis and function in biofilm formation. NPJ Biofilms Microbiomes 7:56.

Koebnik, R., Cesbron, S., Chen, N. W., Fischer-Le Saux, M., Hutin, M., Jacques, M.-A., Noël, L. D., Perez-Quintero, A., Portier, P., and Pruvost, O. 2024. Celebrating the 20th anniversary of the first *Xanthomonas* genome sequences–how genomics revolutionized taxonomy, provided insight into the emergence of pathogenic bacteria, enabled new fundamental discoveries and helped developing novel control measures–a perspective from the French network on Xanthomonads. Peer Comm. J. 4.

Leprevost, L., Jünger, S., Lippens, G., Guillaume, C., Sicoli, G., Oliveira, L., Falcone, E., de Santis, E., Rivera-Millot, A., and Billon, G. 2024. A widespread family of ribosomal peptide metallophores involved in bacterial adaptation to metal stress. Proc. Natl. Acad. Sci. USA 121:e2408304121.

Li, Y., and Rebuffat, S. 2020. The manifold roles of microbial ribosomal peptide–based natural products in physiology and ecology. J. Biol. Chem. 295:34–54.

Luu, D. D., Joe, A., Chen, Y., Parys, K., Bahar, O., Pruitt, R., Chan, L. J. G., Petzold, C. J., Long, K., and Adamchak, C. 2019. Biosynthesis and secretion of the microbial sulfated peptide RaxX and binding to the rice XA21 immune receptor. Proc. Natl. Acad. Sci. USA 116:8525–8534.

Maddock, D., and Hulin, M. T. 2025. From genes to epidemics: Genomic insights into bacterial plant pathogen emergence. Curr. Opin. Plant Biol. 87:102765.
Mareuil, F., Doppelt-Azeroual, O., Ménager, H., Mareuil, F., Doppelt-Azeroual, O., and Ménager, H. 2017. A public Galaxy platform at Pasteur used as an execution engine for web services. F1000Res. 6.
Néron, B., Denise, R., Coluzzi, C., Touchon, M., Rocha, E. P., and Abby, S. S. 2023. MacSyFinder v2: Improved modelling and search engine to identify molecular systems in genomes. Peer Comm. J. 3.
Ogbuji, N. G., and Agogbua, J. U. 2025. Genomics in plant pathogen identification and control. Front. Plant Sci. 16:1661432.
Polidore, A. L., Caserio, A. D., Zhu, L., and Metcalf, W. W. 2024. Complete biochemical characterization of pantaphos biosynthesis highlights an unusual role for a SAM-dependent methyltransferase. Angew. Chem. Int. Ed. 63:e202317262.
Polidore, A. L. A., Furiassi, L., Hergenrother, P. J., and Metcalf, W. W. 2021. A phosphonate natural product made by *Pantoea ananatis* is necessary and sufficient for the hallmark lesions of onion center rot. Mbio 12:10.1128.
Pruitt, R. N., Joe, A., Zhang, W., Feng, W., Stewart, V., Schwessinger, B., Dinneny, J. R., and Ronald, P. C. 2017. A microbially derived tyrosine-sulfated peptide mimics a plant peptide hormone. New Phytol. 215:725–736.
Pruitt, R. N., Schwessinger, B., Joe, A., Thomas, N., Liu, F., Albert, M., Robinson, M. R., Chan, L. J. G., Luu, D. D., and Chen, H. 2015. The rice immune receptor XA21 recognizes a tyrosine-sulfated protein from a Gram-negative bacterium. Sci. Adv. 1:e1500245.
Schöner, T. A., Gassel, S., Osawa, A., Tobias, N. J., Okuno, Y., Sakakibara, Y., Shindo, K., Sandmann, G., and Bode, H. B. 2016. Aryl polyenes, a highly abundant class of bacterial natural products, are functionally related to antioxidative carotenoids. Chembiochem 17:247–253.
Schwengers, O., Jelonek, L., Dieckmann, M. A., Beyvers, S., Blom, J., and Goesmann, A. 2021. Bakta: rapid and standardized annotation of bacterial genomes via alignment-free sequence identification. Microb. Genom. 7:000685.
Shin, G. Y., Dutta, B., and Kvitko, B. 2023. The genetic requirements for HiVir-mediated onion necrosis by *Pantoea ananatis*, a necrotrophic plant pathogen. Mol. Plant-Microbe Interact. 36:381–391.
Shyntum, D. Y., Venter, S. N., Moleleki, L. N., Toth, I., and Coutinho, T. A. 2014. Comparative genomics of type VI secretion systems in strains of *Pantoea ananatis* from different environments. BMC Genom. 15:163.
Straub, C., Colombi, E., and McCann, H. C. 2021. Population genomics of bacterial plant pathogens. Phytopathology 111:23–31.
Timilsina, S., Goss, E. M., Koebnik, R., Potnis, N., and Jones, J. B. 2022. Population and comparative genomics of plant pathogenic bacteria. Front. Microbiol. 13:1012034.
Weller-Stuart, T., Toth, I., De Maayer, P., and Coutinho, T. 2017. Swimming and twitching motility are essential for attachment and virulence of *Pantoea ananatis* in onion seedlings. Mol. Plant Pathol. 18:734–745.
Zhao, X., Gao, L., Ali, Q., Yu, C., Yuan, B., Huang, H., Long, J., Gu, Q., Wu, H., and Gao, X. 2024. A type VI secretion system effector TseG of *Pantoea ananatis* is involved in virulence and antibacterial activity. Mol. Plant Pathol. 25:e13442.

APPENDIX II: SUPPLEMENTARY FIGURES FOR CHAPTER 2

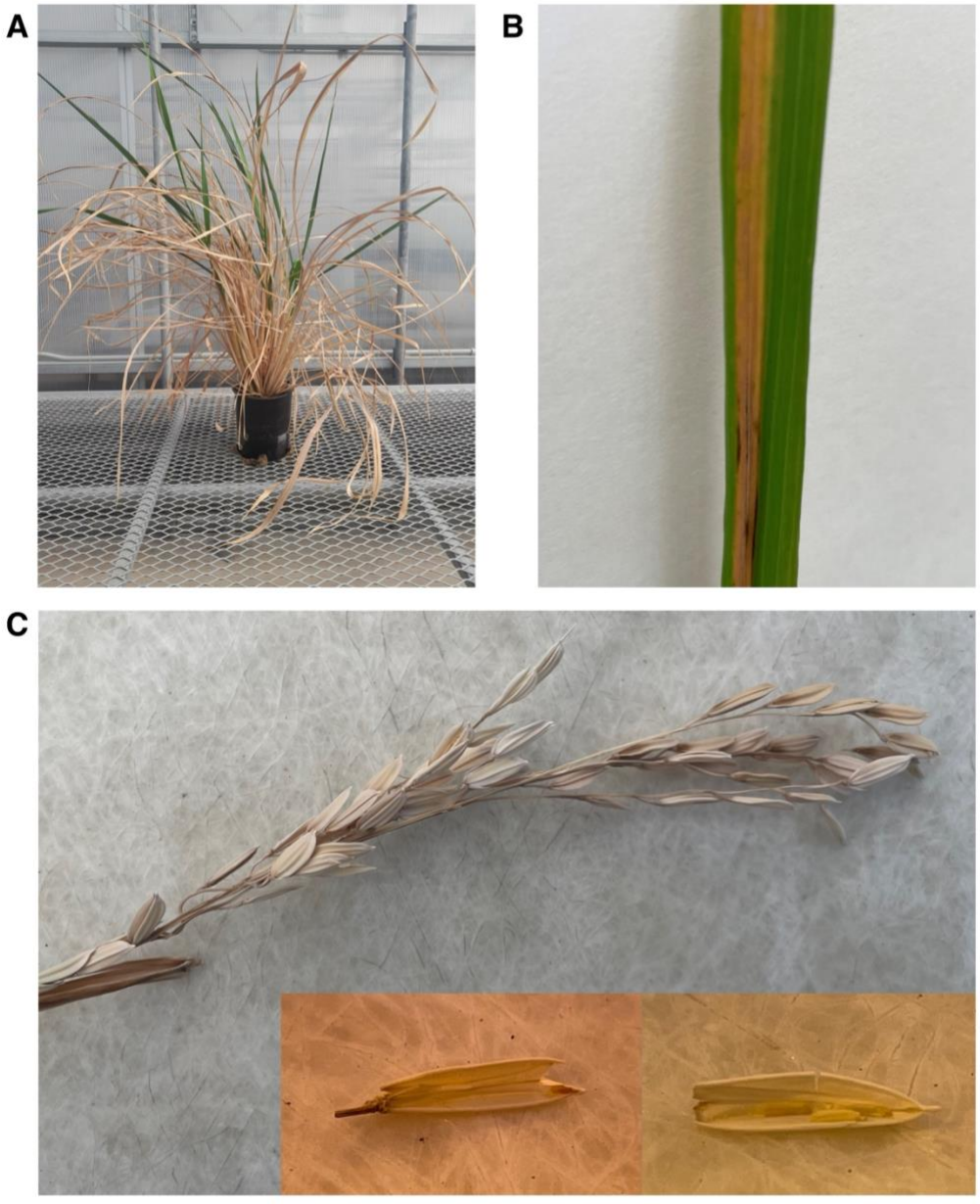


**Fig. S1.** Symptoms of natural infection of *P. ananatis* on rice variety JiBoYa in greenhouse conditions. **A,** Late-stage symptoms resulting in mature JiBoYa. **B,** Bacterial leaf-blight-like symptoms spreading on rice leaf. **C,** Incomplete development of panicle.

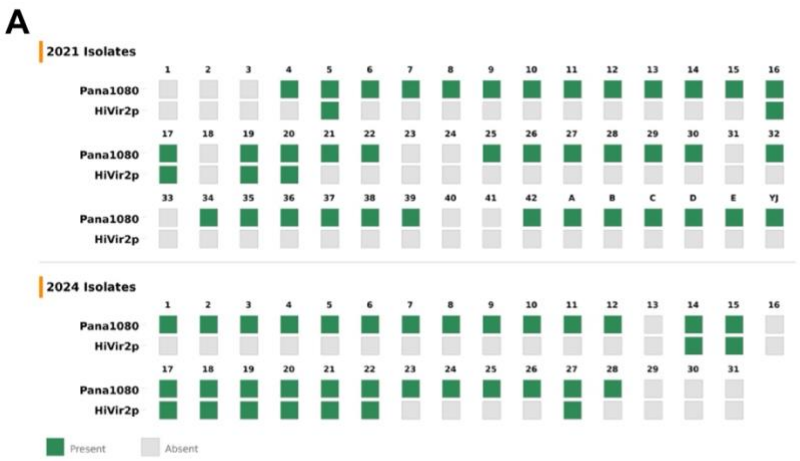


B

| Sequenced strain | Year | Isolate |
|---|---|---|
| AR358 | 2021 | E |
| JEL0889 | 2021 | YJ |
| JEL0890 | 2021 | 10 |
| JEL0891 | 2021 | 16 |
| JEL0892 | 2021 | 20 |
| JEL0893 | 2021 | B |
| PP088 | 2024 | 7 |
| PP092 | 2024 | 12 |
| PP094-PanT1S3 | 2024 | 14 |
| PP099-PanT13S3 | 2024 | 19 |
| PP103 | 2024 | 25 |
| PP105 | 2024 | 27 |

**Fig. S2**. **A,** PCR amplification results on 2021 and 2024 strains of *P. ananatis* isolated from symptomatic rice tissue, including strains sequenced for this study. *P. ananatis* identity was screened with PANA1080 primers (Asselin et al. 2016; Shin et al. 2022), HiVir was screened with HiVri2p primers (Stice et al. 2021). Green indicates amplification; grey indicates no amplification. **B,** Pairing sequenced strain name with original isolate number from the collection of isolates from symptomatic rice tissue.

>PP105 *hvrB*

ATGACCATGAAAAAAAAAGAGATGATAATAGGTGCCTATATATCGTATGGAACAGGACATCATCCTGCTT
CATGGCGCGAAAGTGGCGTAAATGCAGCGGCAGCGCTTGATATTGATACGTATGCCAATCTTGCAAGA
GTATGTGAGAAAGGATTAGCTGATTTACTTTTTCTTGCAGATACGCCTTCTGTATTTCAGGACAATATGG
ACGGTTATGGCAGCAGGGTATCTGTACTGGAGCCATTATCATTATTATCGTATTTAGCATCTCAAACACA
AAATATTGGGCTGGTTGCGACGGCTTCAACGACGTACAAACACCCTTACAACATTGCGAGGGAATTTG
CTTCGCTGGATTACATTAGCAAAGGAAGGGCAGGGTGGAATCTGGTGACATCCTCAAAGTCGGATGC
GGCTAAAAACTTTGGCCTTGCCGCTCATCCAGAACATTCAAAGCGTTATGATATGGCCTGGGAAGCAT
GGCAGGTTATCAGTGGTTTGTGGGACAGCTGGGAAGACAATGCTTTAGTAAGGAATAAAACCAGTGG
ACAATTCTTCGTTAAGGATAAATACCGGGAAATAAATTTTGAGGGTGAATATTTTAATGTAAAAGGCCCA
TTAAACATAGCTCGCCCTCCTCAGGGCTATCCCGTCATCGTCCAGGCGGGTTCCTCTGAGGAAGGAA
AAGAGTTAGCTGCAAAAACAGCAGATATTGTTTTACTGCACAAAACAATATTGAAGATGCAAAAAAATT
CTATGATGATCTTAAAGGGCGAATGGAAAAATACGGAAGGTCAAAGAGTGAACTTCTTATTCTTCCCGG
ATTAAGCTTTTATATTGCAAGTGACGAATCTAAAGCCCGTAAAAAGCTTAATGATCTCAACGCACTGATC
CCTCAATCATTTGGCTTAAGTATGTTATCAGATTTACTGGGTGGGGTTGATTTAAAAAACAATGATCCTG
AAGGACCATTACCAGATTTACCGAAATCTAATGGTAATCAGAGTAGACAAAAAATTATTATCGATTTAGCT
CGAAAAGAAAAACTATCTATCAAGCAACTTTATGAAAAAATAATCATTTCAAGAGGACATTATACATTTAC
AGGTTCCTATCAAGATTTAGCAGATGAGATGATTAAGTGGGTTGAAAATGAAGCATGTGATGGTTTCAA
CATTATGCCTCCTCTCATGCCTGAATCTCTTATTAATCTTTTCGATCATGTCATTCCACTTATTCAGGCAA
GAGGATGGTATAAAAAATCATATTCTACTGGAACATTAAGAGAAAAACTGGGGCTTAAAAGACCTACTA
ATAAATTGTTTAATCAATAA

>PP105 Δ*hvrB*

ATGACCATGAAAAAAAAAGAGATGATAATAGGTGCCCCCGGGAGACCTACTAATAAATTGTTTAATCAAT
AA

>PP105 *hvrF*

ATGAAAAGTGAAAAGTTTGATGGTTTGGCTGATAACTATGATAAATATCGTCCCCGTTATCCTGCAATCG
TTTTCAAGGAAATCCATGACTGGATGCAGCCGTCTGCCAAAAATATATACGATATTGGCGCAGGCACA
GGTATTGCTATTGAAGGTATGACACGTGTCACTGGAAAACACTATGATTTCACGGCGATAGATATTTCT
GAAGATATGATAAAAAAAGGAAGGGAAAAACTGCCTGGTACGACTTGGGTTAAAGGAAAAGCGGAAG
ATATTCTTTCTGATAAAAGCCGTATTGACGTCATTATGGCGGCACAGTCCTTCCAATGGATGGATAGAG
CTAAAACATTAGAAGTTTCGATAAAATCTTTAAATAAGGGCGGGGGTTTTTGCAGTTTTGCAAAACAATCG
AGATTACAGAAATAATGAAATGCTTAACAAATATGAAGGTTTGCTAGAGAAATTTAGTCCAGGTTACAGC
AGACATTATCGCGACTATGACTATGAAAATGAAATCACCAATGTTTTTAAATTGCCTATTGCTAACTTTAA
GAAAGTCGTCACAGGGTGGACTATGGAAATGATTTCAGAAGATTTTTTTGGATTCATTTCTTCCTCAAC
CCAGGTACAAAGAGCTATTGAGAACGATCGTAATGGATTCTGGAAGGAGATTGAAATCTTGATTGACG
AACACTCAGTTGGTGGAAAAATTAGCATAGATTATATAAGTGAGTTATTTATAGCTAAGAAGCGTGATGA
TTCATAG

>PP105 Δ*hvrF*

ATGAAAAGTGAAAAGTTTGATGGTTTGGCTGATAACTATGATAAATATCGTCCCGGGATAAGTGAGTTAT
TTATAGCTAAGAAGCGTGATGATTCATAG

**Fig. S3.** HiVir mutant sequences in PP105. In order, PP105 WT *hvrB* sequence (red indicates what was deleted during allelic exchange), PP105Δ*hvrB hvrB* sequence (green indicates added restriction site), PP105 WT *hvrF* sequence (red indicates what was deleted during allelic exchange), PP105Δ*hvrF hvrF* sequence (green indicates added restriction site).

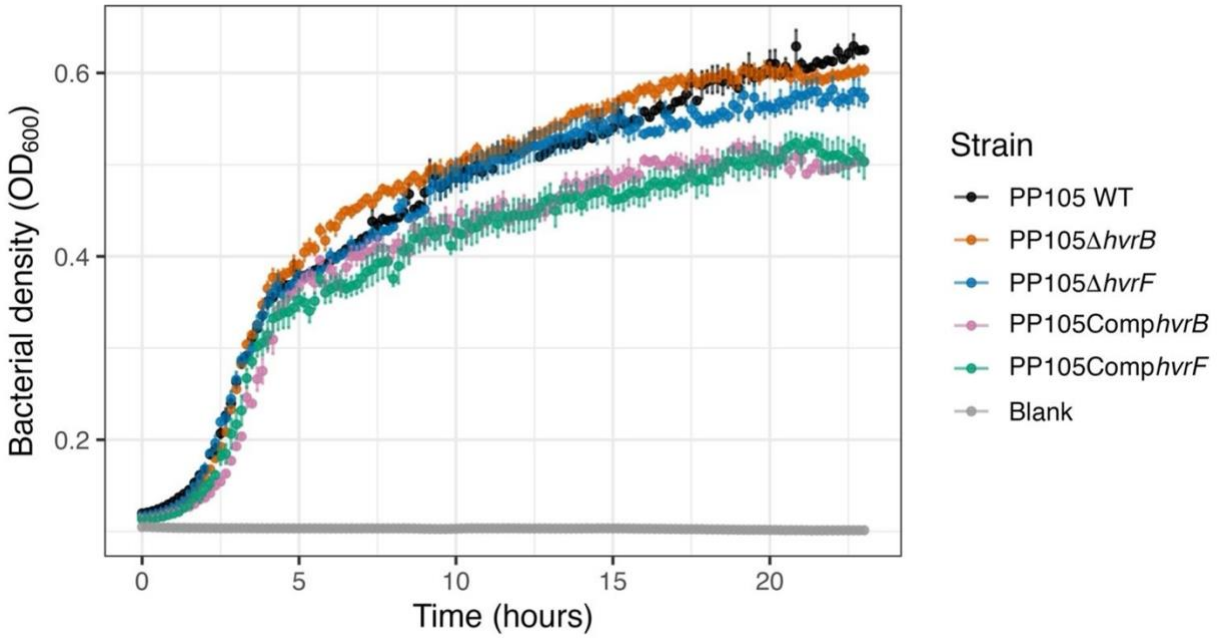


**Fig. S4.** *In vitro* growth curves of WT PP105, mutant strains (PP105Δ*hvrB,* PP105Δ*hvrF*), and complemented strains in liquid LB medium at 30°C with constant shaking. Blank was sterile LB medium.

## REFERENCES

Asselin, J. A. E., Bonasera, J. M., and Beer, S. V. 2016. PCR primers for detection of *Pantoea ananatis*, *Burkholderia* spp., and *Enterobacter* sp. from onion. Plant Dis. 100:836–846.

Shin, G. Y., Smith, A., Coutinho, T. A., Dutta, B., and Kvitko, B. H. 2022. Validation of species-specific PCR assays for the detection of *Pantoea ananatis, P. agglomerans, P. allii*, and *P. stewartii*. Plant Dis. 106:2563–2570.

Stice, S. P., Shin, G. Y., De Armas, S., Koirala, S., Galván, G. A., Siri, M. I., Severns, P. M., Coutinho, T., Dutta, B., and Kvitko, B. H. 2021. The distribution of onion virulence gene clusters among *Pantoea* spp. Front. Plant Sci. 12:643787.